

# SEET: SPACE ENVIRONMENT AND EFFECTS TOOL FOR AGI'S SYSTEMS TOOL KIT (STK)

The document discusses the functionality and options available from Space Environment and Effects Tool (SEET) by Atmospheric and Environmental Research, Inc. (AER) for AGI's Systems Tool Kit (STK).

## INTRODUCTION

AER's Space Environment and Effects Tool (SEET) provides comprehensive modeling of the space environment, with the capability to predict various effects of the ambient near-earth environment on a space vehicle. It provides extensive information on the space environment through which the objects are traveling using the following modules:

- The *Trapped Radiation Environment* module computes the expected ionizing dose rate and energetic particle fluxes experienced by a satellite along its trajectory due to the trapped electron and proton populations, as well as integrated total dose and fluence (flux integrated over time).
- The *Untrapped Radiation Environment* module computes Galactic Cosmic Ray (GCR) differential and integral fluxes and Solar Energetic Particle (SEP) probabilistic fluences over mission lifetimes based on internationally recognized models.
- The *South Atlantic Anomaly Transit* (SAA) module computes the entrance and exit times and probable fluxes for a satellite crossing the SAA, a region of space with an enhanced concentration of ionizing radiation.
- The *Particle Impacts* module computes the probabilistic distribution of small mass particles incident on a spacecraft of a given cross-section and orbit, above a user-specified damage threshold.
- The *Vehicle Temperature* module computes the expected (mean) temperature of a satellite exposed to direct solar and reflected earth radiation, using simple thermal balancing equations.
- The *Magnetic Field* module computes the magnetic field along the satellite path, as well as performing field-line tracing, using standard models.

The models supporting the Radiation Environment, SAA Transit, and Magnetic Field modules have been adapted directly from the Air Force Research Laboratory (AFRL) AF-GEOSpace Version 2.1P software suite. The Particle Impacts module has been adapted from the Meteor Impact module in AF-GEOSpace and extended to include orbital debris.

Most of the SEET modules provide climatological information about the state of the space environment based on the binning and averaging of large amounts of historical data. Climatological information is most useful for satellite designers and mission planners needing to anticipate envi-

ronmental factors over a multi-year mission, or to perform trade studies for different orbits and instrumentation shielding strategies for best and worst-case radiation exposures.

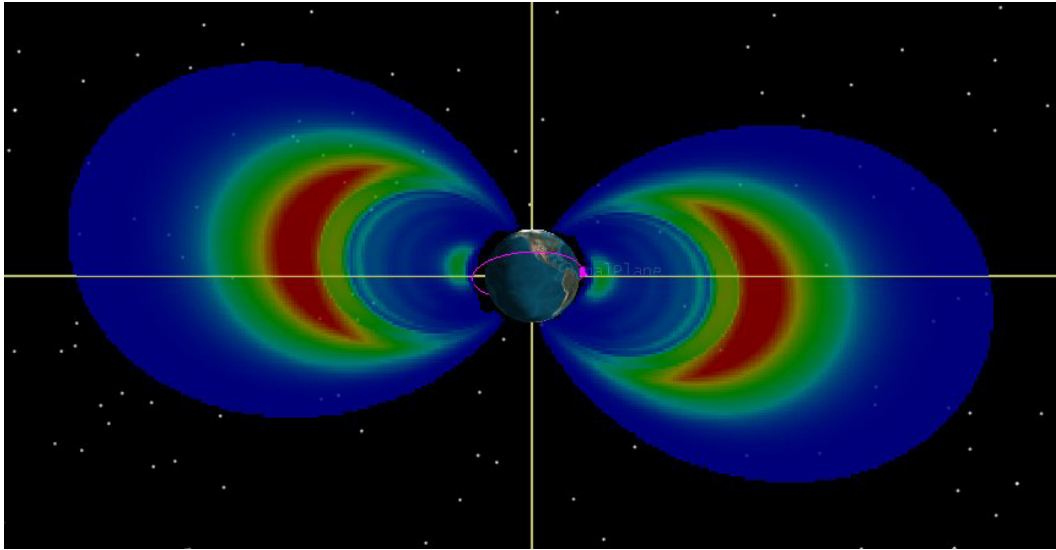


**Figure 1. Electron radiation flux cross-section for particles at 0.95 MeV based on the NASAELE model. Higher values are concentrated in two belts, the Van Allen radiation belts. (Figure courtesy of AER, Inc.)**

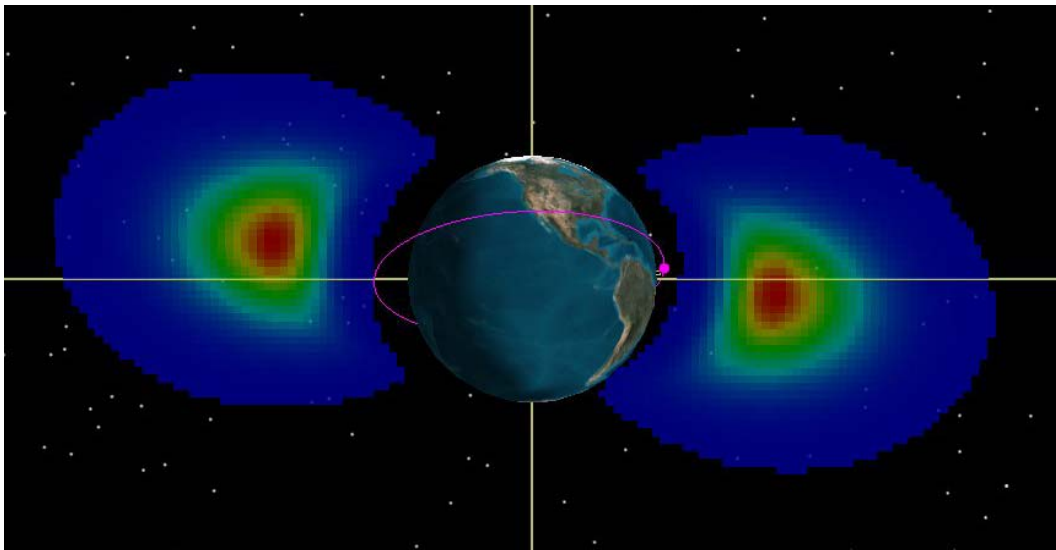


**Figure 2. Proton radiation flux cross-section for particles at 5.7 MeV based on the NASAPRO model. Higher values are concentrated in the inner Van Allen radiation belt. (Figure courtesy of AER, Inc.)**

## **RELEASE NOTES FOR STK-SEET 10.1.1**

The 10.1.1 release of STK-SEET models the Untrapped Radiation Environment by computing Galactic Cosmic Ray (GCR) flux and Solar Energetic Particle (SEP) fluence. For GCR, SEET supports worst-case reporting and graphing of flux versus energy and fluence versus energy spectra over scenario duration using any of three GCR models: CREME86, Badwar-O'Neil 2010 and ISO-15390. SEET supports three SEP models: JPL91, Rosenqvist and Xapsos' ESP model. For these models, SEET also supports worst-case reporting and graphing over scenario duration of fluence versus probability of exceeding fluence at a given energy threshold and energy versus fluence spectrum at a given probability of exceedence.

## **RELEASE NOTES FOR STK-SEET 9.2.3 AND SEET 10**

The 9.2.3 release of STK-SEET provides significant enhancements to the Radiation Environment module. Specifically, the dose computation has been dramatically speeded up by providing the user an option to accumulate flux over a selectable time period prior to computing dose. There is no loss of accuracy in total dose accumulation or in the average dose rate over the reporting time period. User-selectable options are also now provided that allow the CRRES and NASA flux models to behave more like the versions provided by SPENVIS, i.e., by using a fixed-epoch and shifted-SAA magnetic field model approach to computing the L and B/B0 indices into the radiation environment databases (see Heynderickx 1996.) Also, support for integrated flux output has been added to the previously supported differential flux output option. Finally, an extensive cross-comparison of flux model outputs with industry standard implementations, IRBEMLIB (formerly ONERA-Lib) and SPENVIS has been performed and a summary report included as an Appendix to this manual.

An additional magnetic main-field model has also been added; an offset-dipole model based on the IGRF coefficients for the current scenario date and time (as in Fraser-Smith, 1987.)

## **RELEASE NOTES FOR STK-SEET 9.2**

The 9.2 release of STK-SEET provides integration of the IGRF 2010 epoch coefficients into the Magnetic Field module.

## **TRAPPED RADIATION ENVIRONMENT**

Earth's radiation environment is principally composed of naturally occurring charged particles trapped in the Earth's magnetic field in regions known as the Van Allen belts. Solar energetic particles (SEPs) and galactic cosmic rays (GCRs) also contribute to the natural radiation environment. The Van Allen radiation belt particles are responsible for most of the long-term ionizing-dose damage to satellite electronics and materials. GCRs, and SEPs during solar storms, are typically important sources of single event effects (SEEs) and single event upsets (SEUs) that result in instantaneous upsets and glitches in the operation of satellite electronics.

Information on satellite dosage and incident energetic particle flux is important to satellite designers and mission planners because devices on satellites degrade over time due to the collected dose. The total dose is computed by integrating the instantaneous dosage rate over time, where the dosage rate itself depends on the incident energetic particle flux and shielding parameters (material type and thickness) of a shielded instrument.

The SEET *Trapped Radiation Environment* module computes the expected dosage rate and accumulated dose (ionizing energy deposition) due to energetic electron and proton particle flux-

es for a range of user-specified shielding thicknesses. It also computes the energetic proton and electron fluxes for a wide range of particle energies (Figure 1 and Figure 2). The SEET Radiation Environment incorporates the following models from Air Force Research Laboratory's AF-GEOSpace program version 2.1P (AF-GEOSpace User's Manual Version 2.1P, 2006):

*APEXRAD* is a radiation model based on data collected by the APEX Space Radiation Dosimeter to predict the amount of radiation received (dosage rate or total dose), providing dosing data from behind four shielding thicknesses (4.29, 82.5, 232.5, 457.5 mil Aluminum).\*

*CRRESRAD* is a radiation model based on data collected by the Combined Release and Radiation Effects Satellite (CRRES) Space Radiation Dosimeter to predict the amount of radiation received (dosage rate or total dose), providing dosing data from behind four shielding thicknesses (82.5, 232.5, 457.5, 886.5 mil Aluminum).\* The CRRESRAD database is divided into several activity levels: *quiet* refers to data obtained before the large 24-Mar-1991 storm, *active* refers to data obtained after the storm, and *average* refers to the average over the mission.

*CRRESELE* is an electron-flux model that computes the energy differential omni-directional energetic electron flux at discrete energies in the range 0.5-6 MeV, using flux models constructed from data collected by the High Energy Electron Fluxmeter (HEEF) instrument flown on CRRES. It reports electron fluxes only for a specific set of energy levels (0.65, 0.95, 1.60, 2.00, 2.35, 2.75, 3.15, 3.75, 4.55, 5.75 MeV).

*CRRESPRO* is a proton-flux model that computes the energy differential omni-directional energetic proton flux at discrete energies in the range 1-100 MeV, using flux models created from data collected by the proton telescope (PROTEL) flown on CRRES. It reports proton fluxes only for a specific set of energy values (1.5, 2.1, 2.5, 2.9, 3.6, 4.3, 5.7, 6.8, 8.5, 9.7, 10.7, 13.2, 16.9, 19.4, 26.3, 30.9, 36.3, 41.1, 47.0, 55.0, 65.7, 81.3 MeV). The CRRESPRO database is divided into two activity levels: *quiet* refers to data obtained before the large 24-Mar-1991 storm and *active* refers to data obtained after the storm.

*NASAELE* is an electron-flux model that computes the energy differential omni-directional electron flux using the NASA AE-8 radiation belt models at user-specified energies between 0.04 and 7.0 MeV.

*NASAPRO* is a proton-flux model that computes the energy differential omni-directional proton flux using the NASA AP-8 radiation belt models at user-specified energies between 0.1 and 400 MeV.

*SHIELDOSE-2* is a radiation-transport model that uses the electron and proton fluxes computed by the flux models to estimate the absorbed total dose of a detector as a function of depth in a user-specified shielding material (Figure 3). For arbitrary proton and electron incident spectra, the SHIELDOSE-2 model calculates the dose absorbed in small volumes of the detector materials covered by an aluminum shield of user-specified depth. Outputs include total and species dosage rates due to electrons, electron bremsstrahlung, and protons.

---

\* APEXRAD and CRRESRAD do not specifically compute proton or electron fluxes, or provide constituent dosage rate and dose information - only combined information from all constituent sources.

The ranges of the various database models depend upon two parameters derived from the magnetic field model: the McIlwain L-shell parameter ( $L$ , a measure that indicates a particle's drift shell in the magnetic field), and the ratio of the magnetic field strength  $B$  at the current position along a field line to the minimum magnetic field strength at the equator  $B_{eq}$  along the same line, expressed as  $B/B_{eq}$ . The models' ranges of validity, expressed in  $L$  and  $B/B_{eq}$  space, are given in Table 1.

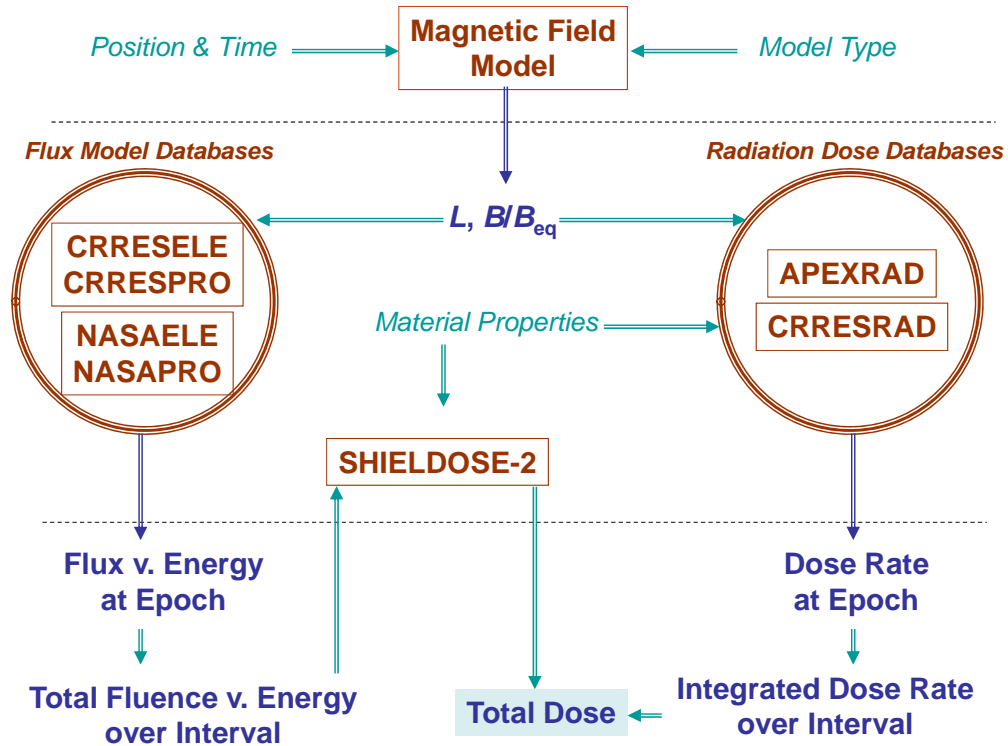


Figure 3. Radiation Environment Model Interdependencies.

Table 1. Ranges of validity of the various radiation environment models

| Mode           | $L$     |         | $B/B_{eq}$ |         |
|----------------|---------|---------|------------|---------|
|                | Minimum | Maximum | Minimum    | Maximum |
| <i>APEXRAD</i> | 1.0     | 5.95    | 1.0        | 13131.5 |
| <i>CRRES</i>   | 1.0     | 8.0     | 1.0        | 7.4     |
| <i>NASA</i>    | 1.17    | 11.5    | 1.0        | 12.0    |

### Computational Modes

The user may access the radiation environment models by selecting one of five major computational modes.

*APEXRAD.* Radiation dose rates and integrated doses only, based on data collected by the APEX Space Radiation Dosimeter for shielding thicknesses of 4.29, 82.5, 232.5, and 457.5 mil Aluminum.

*CRRESRAD.* Radiation dose rates and integrated doses only, based on data collected by the Combined Release and Radiation Effects Satellite (CRRES) Space Radiation Dosimeter for shielding thicknesses of 82.5, 232.5, 457.5, and 886.5 mil Aluminum.

*Radiation Only.* Radiation dose rates and integrated doses only, based on data from both CRRESRAD and APEXRAD; computations default to the APEXRAD radiation models but will use CRRESRAD outside the APEXRAD range of validity (Table 1). Only the common set of shielding thicknesses between APEXRAD and CRRESRAD can be used in this mode (82.5, 232.5, 457.5 mil Aluminum).

*CRRES.* Charged particle fluxes and fluences (fluxes integrated over time), as well as dose rates and integrated doses, from the CRRESELE and CRRESPRO models, are available using all proton and electron energies supported by the CRRES models. Dose computations are performed by using the CRRES model results as input to SHIELDOSE-2.

*NASA.* Charged particle fluxes and fluences, as well as dose rates and integrated doses, from the NASAELE and NASAPRO models, are available using either the CRRES model proton and electron energies, or a user-specified list. Dose computations are performed by using the NASA model results as input to SHIELDOSE-2.

### **User-Selectable SHIELDOSE-2 Model Parameters**

For dose computations in combination with the CRRES or NASA flux models, the SHIELDOSE-2 radiation-transport model is used to estimate ionizing energy deposition (dose). Starting with STK-SEET 9.2.3, a major update has been made to increase the speed of the SHIELDOSE-2 dose rate computations. Specifically, in the Satellite Properties tab under the SEET Radiation menu, the user is allowed to specify both a “Dose Report Step”, indicating the time cadence of dose output during the scenario and a “Dose Integration Step”, indicating the time step for sampling the fluxes that go into the dose computation. Fluxes are accumulated at the time-resolution specified by the Dose Integration Step for a period corresponding to the Dose Report Step, then passed to SHIELDOSE-2 for dose computation. Speed-ups are on the order of Dose Report Step over orbit time-step, e.g., 1440 min/1 min = 1440 for an integration interval of 1 day and orbit time step of 1 minute (assuming Dose Integration Step = orbit time step, which is a reasonable choice.) Since many users are only interested in total annual dose or dose for mission lifetime, longer integration intervals are appropriate and will yield proportionately faster computation times compared to the previous implementation.

When SHIELDOSE-2 is active (via the CRRES or NASA computational modes), the user may specify up to 70 shielding thicknesses, as well as the following options:

*Detector Type.* Users select the type of a small-volume of material specimen under Aluminum shielding to be used for dose computations from the SHIELDOSE-2 radiation-transport model. Detector type options include: Aluminum, Graphite, Silicon, Air, Bone, Calcium, Gallium, Lithium, Silicon Dioxide, tissue, and water. The default detector type is Silicon.

*Shielding Geometry.* Users select the geometry of a material specimen under Aluminum shielding to be used for dose computations from the SHIELDOSE-2 radiation-transport model. Detector geometry options include:

- *Finite-slab*: The detector is embedded in one side a planar slab of Aluminum shielding material, and is irradiated through the slab from the other side.
- *Semi-infinite slab*: The detector has the same geometry as the finite slab, except that the Aluminum shielding material has no boundary behind the irradiated surface (thereby enclosing the detector material).
- *Spherical*: The detector is embedded at the center of a solid sphere of Aluminum and irradiated from all directions.

*Nuclear Attenuation Mode.* Users select the degree of nuclear attenuation for dose computations from the SHIELDOSE-2 radiation-transport model. Possible values are *nuclear attenuation* (due to local charged secondary energy deposition), and *nuclear attenuation plus neutrons*.

A matrix of user-selectable model parameters affected SHIELDOSE-2 radiation-transport model is shown as Table 2.

**Table 2. Matrix of User-Selectable Model Parameters Affecting Various SEET Modules**

|                             | <i>Radiation Only Mode</i> |                 | <i>CRRES Mode</i> |                 | <i>NASA Mode</i> |                |
|-----------------------------|----------------------------|-----------------|-------------------|-----------------|------------------|----------------|
|                             | <i>APEXRAD</i>             | <i>CRRESRAD</i> | <i>CRRESPRO</i>   | <i>CRRESELE</i> | <i>NASAPRO</i>   | <i>NASAELE</i> |
| Flux Output<br>Energy Lists |                            |                 |                   |                 | ✓                | ✓              |
| Ap Flux<br>Source           | ✓                          |                 |                   | ✓               |                  |                |
| Dose<br>Channel             | ✓                          | ✓               |                   |                 |                  |                |
| NASA<br>Activity<br>Level   |                            |                 |                   |                 | ✓                | ✓              |
| CRRES<br>Activity<br>Level  |                            | ✓               | ✓                 |                 |                  |                |
| Detector<br>Type            |                            |                 | ☑                 | ☑               | ☑                | ☑              |
| Detector<br>Geometry        |                            |                 | ☑                 | ☑               | ☑                | ☑              |
| Nuclear<br>Attenuation      |                            |                 | ☑                 | ☑               | ☑                | ☑              |

✓ Affects the indicated flux model.

☑ Affects SHIELDOSE-2 when used with the indicated flux model.

## Other User-Selectable Model Parameters

The following user-selectable model parameters are also available for use with the appropriate corresponding computational mode.

*Energy lists for flux output.* These are user-adjustable lists of energies (in MeV) at which to compute the electron and proton fluxes from the NASA models. The energy lists default to the CRRES mode fixed lists, which can be changed from the scenario properties page. The energy lists affects the NASAPRO and NASAELE models (via the NASA computational mode).

*Ap Flux Source.* The input value is a 15-day average of the standard Ap geomagnetic activity index. Source can either be *static value* or *use flux file* to read values from a file. This parameter affects the CRRESELE (via CRRES mode) and APEXRAD (via APEXRAD or Radiation Only computational modes).

*CRRES Activity Level.* Options are *quiet*, *active* (CRRESPRO and CRRESRAD), and *average* (CRRESRAD only). The *quiet* option references data obtained from 27 July 1990 to 19 March 1991 (before the large 24-Mar-1991 storm), *active* references data obtained from 31 March 1991 to 12 October 1991 (after the storm), and *average* references the average of data taken over the entire mission. These different options may be used to give best and worst case dose rates for a given scenario.\* The activity level affects the CRRESPRO model (via CRRES mode) and CRRESRAD model (via CRRESRAD or Radiation Only computational modes), and is set from the scenario properties page.

*NASA Activity Level.* Options are *Solar Minimum* and *Solar Maximum*, the choice of which sets values appropriate for either the minimum or the maximum of the solar cycle while operating within the NASA computational mode. The activity level affects the NASAPRO model and NASAELE model (via the NASA computational modes), and is set from the scenario properties page.

*Dose Channel.* For the purposes of estimating single-particle upset effects (including latch-up), the measured heavy ion flux distributions as a function of particle type and energy are transformed into distributions as a function of the ion's linear energy transfer (LET). The LET is the energy lost by an ion and deposited into the target material per unit distance along the ion's path. Therefore, the user may selectively obtain dose output from three LET regimes: Low LET (0.05-1 MeV deposited from electrons, bremsstrahlung, and proton energies greater than 100 MeV), High LET (1-10 MeV deposited from protons with energies within 20-100 MeV and electrons energies greater than 5 MeV), and Total (0.05 – 10 MeV deposited, the sum of Low LET and High LET). The dose channel affects the CRRESRAD model (via CRRESRAD or Radiation Only computational modes) and the APEXRAD model (via APEXRAD or Radiation Only computational modes).

---

\* Kerns and Gussenhoven (1992) notes that orbits with apogees near geosynchronous altitudes may show a higher dose rate when using the average model than using the active or quiet models because the average model is the only model to use the period between 19 March 1991 and 31 March 1991 during which a strong solar proton event occurred.



Starting with STK-SEET 9.2.3, the following options have been added to this panel; they apply to all models:

*Set magnetic field epoch to Mode's reference epoch.* When this option is selected, the field model used for computing indices into the radiation model databases is set to use the fixed epochs and external field models from which those databases were constructed, as recommended in [Heynderickx, 1996]. The epochs per model are: APEXRAD, 1996, no external field; CRRES models, 1985, Olsen-Pfitzer quiet external field; NASAELE and NASAPRO at solar min, 1962, no external field; NASAPRO at solar max, 1970, no external field. All cases use the IGRF/DGRF main-field model with the corresponding epoch coefficients.

*Shift SAA using Mode's reference epoch.* This switch is only available if the “Set magnetic field epoch to Mode's reference epoch” switch has been selected. In this case, the method of [Heynderickx, 1996] is used to shift the relative location of the effect of the SAA on the magnetic field computation.

Note that the above options only affect the epoch year of the magnetic field computations used internally by the radiation environment models; day-of-year and UT for the internal field computations are unchanged from those of the scenario and nothing outside of the scope of the radiation environment computations is affected at all.

A matrix of the user-selectable model parameters affecting various SEET modules is shown as Table 2.

## **UNTRAPPED RADIATION ENVIRONMENT**

The near-Earth untrapped radiation environment consists of Galactic Cosmic Rays (GCR) originating in inter-stellar space and partially shielded by the solar magnetic field and Solar Energetic Particles (SEP) originating from the Sun through solar flares and coronal mass ejections (CMEs). These highly energetic particles can cause major disruptions to human technology (Feynman & Gabriel, 2000) and pose health risks to astronauts, as well as passengers and crew on polar flights (Beck et al., 2005; Getley et al., 2005). The GCR flux is continuous but relatively low—a few particles per  $\text{cm}^2$  per second. SEPs occur sporadically throughout the solar cycle; they typically last for several days but can reach peak fluxes of tens of thousands of particles per  $\text{cm}^2$  per second. Both GCRs and SEPs consist of protons and heavy ions. The heavy ions (high  $Z$  particles) are particularly effective at causing single-event effects (SEE) in microelectronics and enhanced biological effects.

### **Galactic Cosmic Ray Models**

Galactic cosmic rays (GCR) are high energy charged particles originating from beyond the solar system (Bourdarie and Xapsos, 2008; Xapsos *et al.*, 2013). They consist primarily of atomic nuclei that have been completely stripped of electrons. There is also a so-called anomalous cosmic ray component, or ACR, which is accelerated within the solar system at the shock where the solar wind meets interstellar space. Number fluxes are dominated by protons and alpha particles, but all naturally occurring elements up through uranium are present. Fluxes tend to peak at around 1 GeV per nucleon. For energies below about 10 GeV per nucleon, fluxes are attenuated by the solar magnetic field and the solar wind.

SEET provides three different options for GCR models: CREME86, ISO-15390, and Badhwar-O'Neill 2010. The primary differences among the models are the amount of data on which the model is based and the way they model the solar modulation. All three models calcu-

late particle fluxes in free space outside the Earth's magnetosphere; no geomagnetic cutoff effects are currently applied. Therefore, the models should only be applied to locations at geosynchronous orbit or beyond; application to other orbits will result in an upper limit to the GCR fluxes. SEET output for GCRs currently consists only of reports and graphs and no 2D or 3D graphics. The three models are discussed briefly below.

*CREME86*. The Cosmic Ray Effects on Microelectronics, or CREME86 model (Adams, 1987), was one of the first comprehensive models of GCRs. Energy spectra are based primarily on measurements of hydrogen and helium in the energy range 10 MeV/n to 100 GeV/n. For most other elements, fluxes are scaled from the helium spectrum using either a constant or energy-dependent factor. The solar cycle modulation is modeled as a sinusoidal variation with solar minimum in February 1975 and solar maximum in August 1980. Because the sinusoidal variation is not representative of the true solar-cycle modulation, CREME86 should only be used for the solar extrema, which results in calculated flux values being constant over time.

CREME86 can also include anomalous cosmic rays (ACRs). The model has options to assume whether the ACRs are singly- or fully-ionized via the Interplanetary Weather Index M:

- M=1 (default): This option provides best approximation to the galactic cosmic ray flux at the given date.
- M=2: The “anomalous” component, assumed fully ionized, is added to galactic cosmic rays.
- M=3: This option gives worst-case galactic cosmic ray fluxes that allow uncertainties in flux data and solar activity. These fluxes are so severe that they have only a 10% chance of being exceeded by actual fluxes at any moment.
- M=4: A singly-ionized "anomalous component is assumed. The singly-ionized particles are affected differently than fully-ionized particles by geomagnetic cutoff.

*ISO-15390*. The ISO-15390 model (ISO, 2004; Nymmik, 2000) has been adopted as an international standard for computing GCR spectra. GCR spectra are based on measurements available up until about the year 2015. The model uses multi-parameter fits to relate the solar modulation to observed sunspot numbers. These fits account for the time lag between solar activity and the GCR flux at Earth; this time lag varies between about 8 and 15 months and depends on the phase and polarity of the solar magnetic field and on the magnetic rigidity of the particles. The ISO model is date specific and results in time dynamic flux values.

*Badhwar-O’Neill 2010*. The Badhwar-O’Neill 2010, or BO10 (O’Neill, 2010) includes measurements of GCR flux from 1955 to 2010, spanning Solar Cycles 19 to 24. It is an improvement to the Badhwar-O’Neill 1996 model (Badhwar and O’Neill, 1996). The measurements are heavily based on data from the NASA Advanced Composition Explorer (ACE) Cosmic Ray Isotope Spectrometer (CRIS), measuring the low-energy (50-300 MeV/n) spectrum for all ions from lithium to nickel.\* BO10 uses functions similar to those in ISO-15390 to determine the solar modulation.

*SEET GCR Options*. The primary output for GCR is the flux spectrum (GCR flux versus energy) or total fluence spectrum outside the magnetosphere for a full scenario. This represents a maximal estimate for orbits below geosynchronous altitude, since geomagnetic shielding (rigidity) is not computed. Solar modulation is based on the dates of the scenario or the user provided PHI parameter for BO10. The options available for obtaining GCR fluxes in SEET include the following:

- Model choices: CREME86, ISO-15390, or BO10.
- Atomic Number: Elements from 1 (Hydrogen) to 92 (Uranium) are available in all three models.
- Solar Influence: Options for BO10 are “Solar Min” (corresponding to PHI = 450) and “Solar Max” (corresponding to PHI = 1100). Options for CREME86 include “Solar Min”

---

\* <http://www.srl.caltech.edu/ACE/>

and “Solar Max” by calculating the solar cycle modulation for given dates based on built-in parameters. This option is disabled for ISO15390.

- Interplanetary Weather Index M: This option is only available for CREME86.
- Solar Modulation Parameter  $\Phi$  (PHI): The value of  $\Phi$  used to compute the modulation for the BO10 model is displayed. “Solar Min” corresponds to  $\Phi = 450$  and “Solar Max” corresponds to  $\Phi = 1100$ .
- GCR sample time: This is how often the GCR computation should be called, and defines the cadence of the flux spectral output. The sample time is input as fractional years; the default is 0.25. If the sample time requested exceeds the scenario time range, only one spectrum is returned.

### **Solar Energetic Particles**

Solar Energetic Particles (SEPs) are protons and ions that originate in the solar wind. These particles pose a hazard to orbiting spacecraft (Feynman and Gabriel 2000, Dyer et al. 2004), particularly through internal charging of electronic components. During highly active years in the 11-year solar cycle, there is an increase in SEP flux driven by solar flares and shocks. Solar minimum years, meanwhile, produce low SEP levels. As implemented, these models produce fluences based on the fraction of mission time spent in the seven years around solar max. Short mission lifetimes during solar minimum years may produce zero fluence results.

Using the database of particle observations from the Interplanetary Monitoring Platform (IMP) satellites and Geostationary Operational Environmental Satellites (GOES), models have been developed to predict the cumulative particle fluence expected during the lifetime of a mission. Among these, the (Rosenqvist *et al.*, 2005, Glover et al., 2007), an update to the JPL-91 model, and Emission of Solar Protons (ESP; *e.g.*, Xapsos *et al.*, 1999, 2000) models are implemented in SEET. Descriptions of the models are as follows:

*JPL-91 model.* In the JPL-91 model, (Feynman *et al.*, 1990) characterized expected proton fluence for satellite design using observations obtained between 1963 and early 1991. Data were used from the Interplanetary Monitoring Platform (IMP) 1, 2, 3, 5, 6, 7, and 8 satellites, in addition to OGO 1. The estimate of total proton fluence during a mission is dominated by the probability of the occurrence of large events, associated with solar maximum years. The probability of a proton fluence being exceeded is characterized by a Poisson distribution. The main parameter of importance is the average number of events occurring during the mission.

*Rosenqvist et al. (2005, 2007) model.* As an update to the JPL-91 model, the Rosenqvist *et al.* model includes data from the GOES satellites, with observations from January 1974 to May 2002. Updates were made to the mean and standard deviation of the probability distributions, as well as estimates of the average number of events expected during active years.

*ESP model.* The ESP model uses a maximum entropy technique to determine the probability distribution for exceeding a fluence level during a mission. The data source includes three complete solar cycles (20-22) of proton observations, with data from IMP 3, 4, 5, 7, and 8, as well as GOES 5, 6, and 7. Predictions are made for proton fluence from integral energy channels from  $>1$  MeV through  $> 100$  MeV. Additionally, this model includes a formulation of the worst case event fluence expected.

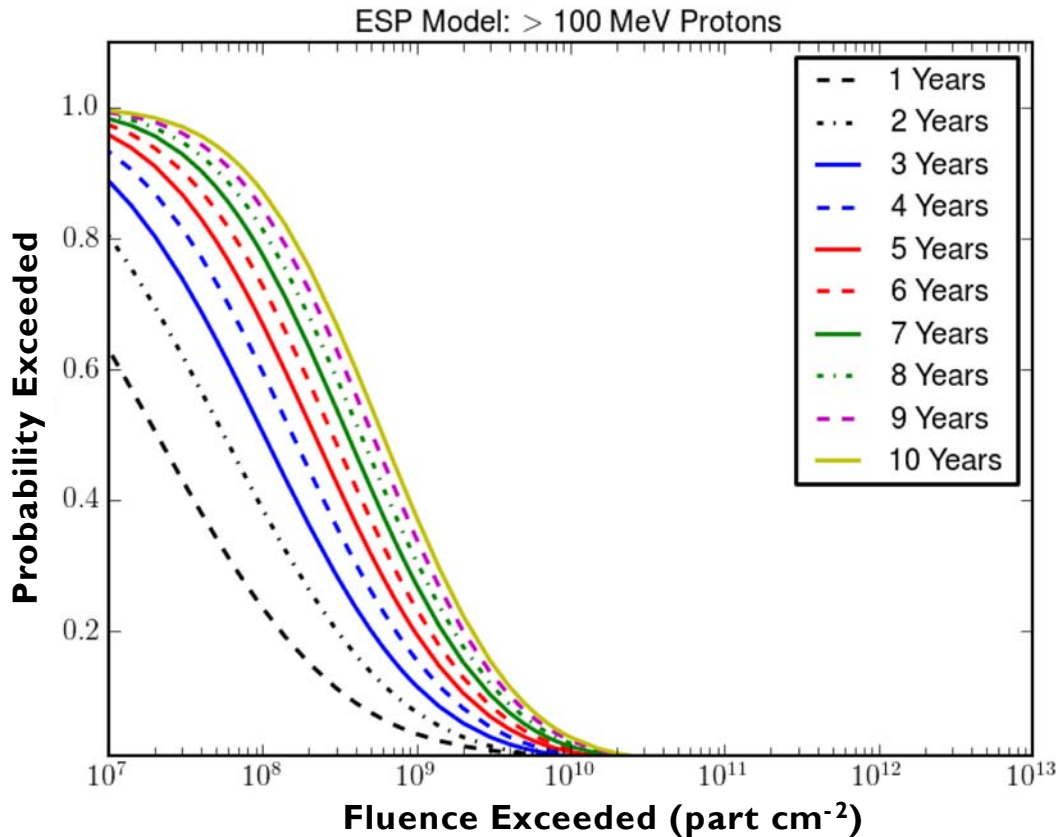


**Figure 4. Probability of exceeding proton fluence level for a variety of mission lengths with the ESP model.**

*SEET SEP Options.* The primary outputs for SEP are the estimated fluence spectra or fluence probability curves for user specified energies, outside the magnetosphere for a full scenario. This represents a maximal estimate for orbits below geosynchronous altitude, since geomagnetic shielding (rigidity) is not computed. The options available for obtaining SEP fluences in SEET include the following:

- Model choices: JPL-91, Rosenqvist, or ESP.
- Mission Duration: Time interval over which the SEP model determines probabilistic thresholds for the fluence level. Valid from 1.0 to 22.0 years inclusive.
- Energies: Energy bin list in MeV for which Fluences to Exceed for specified probabilities will be computed. Entries may be deleted from the default list, but new list entries cannot be added.
- Report probability: This defines the probability threshold for producing the fluence-energy spectrograms. A 95% report probability means that the highest fluence for which the probability of occurrence exceeds 95% will be returned. Note that if a 95% confidence is

required, the fluence won't exceed the values returned; one must specify 5% report probability.

### **SOUTH ATLANTIC ANOMALY (SAA) TRANSIT**

The SAA is a region of space with an increased concentration of ionizing radiation due to the configuration of the Earth's magnetic field. Such radiation can damage spacecraft electronics and cause single event upsets (SEUs) that can impair the functioning of electronic components. Knowledge of when a satellite will be in the SAA is useful for mitigating the risk of damage to spacecraft electronics.

At low altitudes, the Earth's magnetic field is approximately a tilted dipole pattern. Energetic electrons and protons trapped in this field form the Van Allen Belts. Because the center of the magnetic dipole pattern is offset from the center of the Earth, a portion of the inner radiation belt is closer to the Earth in the South Atlantic region than elsewhere; therefore, this region is known as the South Atlantic Anomaly (SAA). At lower altitudes, SAA radiation is concentrated off the South Atlantic coast of Brazil at an altitude of approximately 350 km, with a latitudinal spread of approximately 30° and a longitudinal spread of approximately 60°. With increasing altitude, the SAA region spreads eastward and westward until at approximately 1300 km altitude it completely encircles the Earth (Figure 5).

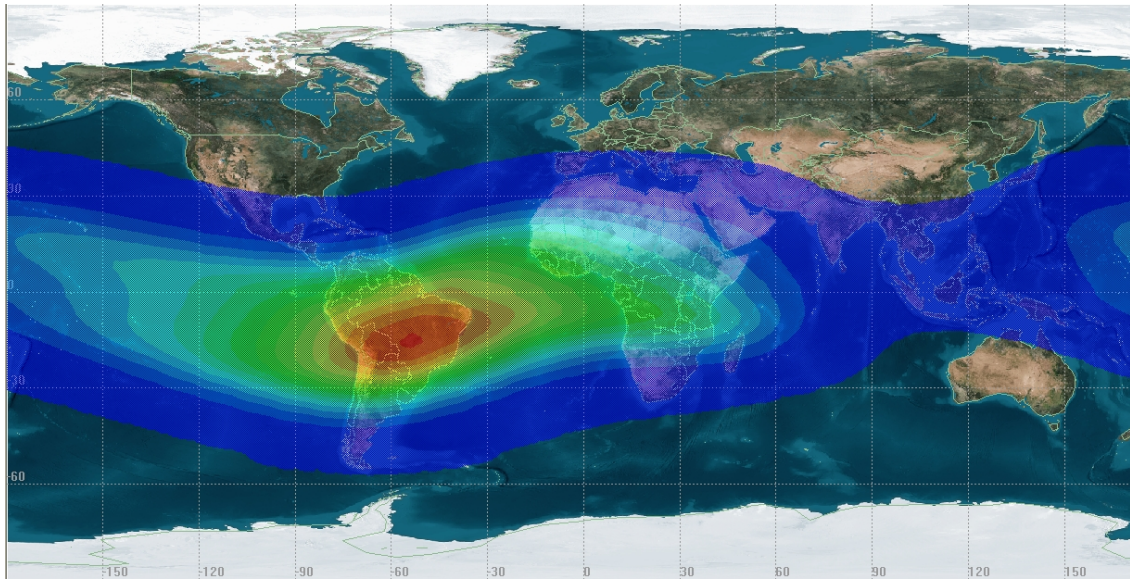


**Figure 5. The South Atlantic Anomaly.  
Flux intensity values at 1650 km altitude for protons > 23MeV.**

The SAA model in SEET is based on data from the Compact Environment Anomaly Sensor (CEASE) proton-telescope detector flown on the Tri-Service Experiment (TSX-5) satellite during the epoch 2000 – 2006 (Ginet *et al.*, 2007). The database, provided by the Air Force Research Laboratory (AFRL), consists of four sets of gridded integral energy flux values above each of four proton-energy flux thresholds; 23, 38, 66, and 94 MeV. The resolution of the data is 3 degrees for both latitude and longitude and 50 km in altitude, covering all latitudes and longitudes and ranging in altitude from 400 km through 1700 km.

SEET's *South Atlantic Anomaly (SAA) Transit* module computes the entrance and exit times of a given satellite through the SAA region, as well as the energy flux as a function of location. All flux-related output requires that the energy channel parameter (one of the four proton-energy thresholds) be specified; the user should select the appropriate energy channel (23, 38, 66, or 94 MeV) based on the nature and sensitivity of on-board instrumentation. Additionally, the model provides methods for retrieving SAA flux contours for specified energy channels and altitudes. The retrieved contour levels are mapped with respect to the maximum flux encountered for the particular energy channel and altitude; the contours that can be requested are *background flux level plus 3 standard deviations*, *tenth of maximum flux*, or *half of maximum flux*.

## **PARTICLE IMPACTS**

SEET's *Particle Impacts* module computes the probable number of small particles impacting a spacecraft along its orbit during a specified time period for particles originating from two environmental sources: naturally occurring meteoroids and man-made orbital debris. The probable number of particles impacting can either be the total number or only those that would cause damage above a surface damage threshold level (pitting depth) specified by the user. Impact by these particles can cause significant damage to space vehicles when the total momentum (mass times relative velocity) of the impacting particles is large. The probable impact rate on a satellite is determined from the modeled particle environment (discussed below) and the cross-sectional area of the satellite (specified by the user). For impacts above the damage threshold, the type of surface material also plays a role and may be specified by the user. The probable total mass distribution of impacting particles may also be computed.\*

### **Meteor Environment**

Annual meteor showers occur when the Earth passes through the dust trails of the various cometary orbits. The timings of these showers are generally well established, though some irregular periods also occur. Most meteoroids consist of particles that have masses in the range 1  $\mu\text{g}$  – 10 mg with a peak near 10  $\mu\text{g}$ . Velocities can range between 12 km/s and 70 km/s. Two important characteristics of meteor showers are the radiant (the point in the sky where meteors from a specific shower seem to come from) and the Zenithal Hourly Rate (ZHR) – the number of shower meteors per hour an observer would see under a clear sky. Generally, the known showers are relatively weak, corresponding to a ZHR of 200 or less. However, occasionally a meteor storm occurs when the Earth passes through an unusually dense cometary dust trail. In those cases, the ZHR may be as high as 10,000 or more for a short time.

SEET's Meteor Environment model is largely based on a database of 50 parameterized annual meteor showers. This database is derived from a table of ten years of visual observations in both northern and southern hemispheres (Jenniskens, 1994). The Jenniskens database specifies each shower in reference to its date and level of its ZHR peak and radiant location. Algorithms are used to translate the database's visual meteor-shower observation rates to mass-dependent flux

---

\* The probable total mass distribution of impacting particles should be used with caution since damage rates will depend on the momentum distribution of the impacting particles and the total mass collected is likely to be negligible.

rates, producing a time-dependent anisotropic meteoroid flux model of 221 different particle types ranging in mass from  $10^{-9}$  g to  $10^2$  g. (McNeil, 1999; McNeil, 2001; Rendtel *et al.*, 1995; Hughes, 1975). The modeled meteoroid flux environment is supplemented with an optional background flux due to *sporadic meteors* (interplanetary cosmic dust that is not associated with any particular meteor shower or source direction) using a commonly-used particle mass distribution profile (Love and Brownlee, 1993; Rendtel *et al.*, 1995).

### **Debris Environment**

Orbital debris consists of large cataloged trackable space objects (such as inactive satellites and spent rocket stages) and the numerous small objects originating from larger space objects (generated by accidental or deliberate explosions, collisions, fragmentations and surface erosion). While large space objects are best modeled as points in space, the smaller objects are best modeled as a spatial distribution of particle size density in space and not as individuals. The spatial distribution and motion of the debris about the Earth is largely dependent on the orbital characteristics of the original parent body and the forces involved in its breakup.

SEET's Debris Environment model is based on the empirically-derived equations by Kessler (1989) that calculate the amount of the small orbital debris particle flux at a given time as a function of particle size, satellite average altitude,\* orbital inclination, and the average of the F10.7 solar activity index for the previous 13 months (the F10.7 index is an indicator of the amount of solar energy affecting the Earth's atmosphere extending back to 1947). This model includes portions that predict the general increase of space debris over time via a fixed annual net growth rate. An average impact velocity profile, as a function of orbital inclination, has been calculated from associated equations. These equations have been based on many years of general debris observations (both space- and Earth-based), and produce yearly-averaged debris-particle flux values.

Given the debris and/or meteoroid flux environment as defined by these models, the algorithms from McDonnell and Sullivan (1991) are used by the Debris Environment module to determine the amount of the particle flux that would be capable of causing damage to a user-specified satellite surface.

### **VEHICLE TEMPERATURE**

SEET's *Vehicle Temperature* module computes the mean equilibrium temperature of a spacecraft due to direct solar and reflected Earth radiation using simple thermal balancing equations (Tribble, 1995). SEET treats the spacecraft as a single isothermal node to determine the steady-state temperature, where the user specifies bulk thermal characteristics of the spacecraft. The temperature computations are based on models for either spherical objects, or planar objects with a specified orientation.

---

\* The Debris Environment module cannot be applied to a spacecraft for which the average altitude is less than 300 km or more than 2250 km.



## Spacecraft Energy Budget

Incoming radiation from the Sun or Earth can be either absorbed or reflected by opaque spacecraft material. Sources of emitted and absorbed energy, along with any internal heat-dissipation, must be accounted for when determining a spacecraft's thermal management system. Conservation of energy under thermal equilibrium requires that

$$Energy_{\text{absorbed}} + Energy_{\text{dissipated}} = Energy_{\text{emitted}} \quad (1)$$

Here, positive energy *dissipation* refers to the radiation of internally produced heat energy resulting from the operation electrical or mechanical components. The total thermal radiation transferred into and out of a spacecraft will be a function of an object's surface reflectivity and emissivity, surface area, temperature, and geometric orientation with respect to other thermally participating objects. *Absorptivity* is the material property that represents the fraction of the incoming radiation that is absorbed (not reflected) by the material, independent of the incident angle of the radiation with the surface, while *emissivity* is the material property that represents the fraction of energy emitted relative to an ideal blackbody at the same temperature.

Using the conservation of energy from Eq. (1) with the Stefan-Boltzmann law, the average external temperature  $T_0$  of a spacecraft may be modeled as

$$\sigma_B T_0^4 = \left[ \left( \frac{(Q_{Sun} + Q_{ER})\eta_0 + Q_i}{\epsilon_0} \right) + Q_{IR} \right] \frac{1}{A_0} \quad (2)$$

where  $\sigma_B$  is the Stefan-Boltzmann constant,  $Q_{Sun}$  is the direct thermal power from the Sun,  $Q_{ER}$  is power due to sunlight reflected from the Earth,  $Q_{IR}$  is radiant infrared power emitted from the Earth due to its temperature,  $Q_i$  is power from heat produced by instrumentation inside the spacecraft,  $\eta_0$  is the material absorptivity of the spacecraft,  $A_0$  the total radiating surface area, and  $\epsilon_0$  is the surface emissivity of the spacecraft. All power sources contribute while the spacecraft is sunlit, but only the emissive-infrared component from the Earth  $Q_{IR}$  and internally-generated heat  $Q_i$  contribute while the spacecraft is in the shadow of the Earth.

## Earth's Infrared Radiation

The Earth's atmosphere, cloud cover, and gas concentrations determine the absorbed portion of the incoming energy and emitted infrared energy. The *albedo* of the Earth is modeled the hemispherical average of the fraction of (visible or short-wavelength) solar energy reflected from the Earth back into space by the Earth's atmosphere, clouds, oceans, ice, and land surfaces. Typically 30% of solar energy at optical wavelengths may be reflected and thereby contribute to  $Q_{ER}$ . The remaining solar energy is absorbed by the atmosphere and Earth's surfaces, raising the Earth's temperature and thereby contributing to  $Q_{IR}$ . The Earth's albedo, the power per unit area from the Sun ("solar constant"), and the spacecraft's distance from the Earth and Sun are therefore used in combination to estimate the radiated power affecting the temperature of the spacecraft. The expression for  $Q_{ER}$  affecting a sphere can be found in Cunningham (1961) and the expression for  $Q_{ER}$  affecting a plate can be found in Cunningham (1963). The expression for  $Q_{IR}$ , also a function of the distance from the Earth and Earth albedo, can be found in Stevenson and Crafton (1961) for both a sphere and a plate.  $Q_{Sun}$  is a function of solar flux, the model shape, and distance from the Sun (Griffin and French, 1991).

To determine the reflected incidence of incoming radiation, the user specifies a plate model or sphere model via the Shape Model parameter, depending on which shape best represents the

spacecraft or spacecraft component to be analyzed. The cross-sectional area for a sphere or plate is also required, and a surface normal vector must be specified for the plate orientation, if applicable. The surface normal vector is defined as the orthogonal vector to the surface, pointing away from the planar surface.

## MAGNETIC FIELD

The Earth's internal magnetic field (*i.e.*, the geomagnetic main field) can be represented approximately as a magnetic dipole, with one pole near the geographic North Pole and the other near the geographic South Pole. The locations of the poles and the strength of the field vary over time, so standard coefficients that represent the geomagnetic field are adjusted periodically. These standard series of coefficients, together with their standard mathematical description, are known as the International Geomagnetic Reference Field (IGRF). The full description of the IGRF main field is a multi-pole spherical harmonic expansion containing over 100 coefficients:

$$V(r, \theta, \lambda, t) = R \sum_{n=1}^{N_{\max}} \left( \left( \frac{R}{r} \right)^{n+1} \sum_{m=0}^n \left( g_n^m(t) \cos(m\lambda) + h_n^m(t) \sin(m\lambda) \right) P_n^m(\theta) \right) \quad (3)$$

where  $r$ ,  $\theta$ ,  $\lambda$  are geocentric coordinates,  $r$  is the distance from the centre of the Earth,  $\theta$  is the co-latitude, (*i.e.*  $90^\circ$  minus latitude), and  $\lambda$  is the longitude,  $R$  is the IGRF reference radius (6371.2 km),  $g_n^m(t)$  and  $h_n^m(t)$  are the harmonic coefficients at time  $t$ , and  $P_n^m(\theta)$  are the Schmidt semi-normalized associated Legendre functions of degree  $n$  and order  $m$ .

The standard coefficients of the IGRF main-field are maintained in tables having nodal values added about once every five years. Between these nodal epochs, the coefficients are linearly interpolated to approximate their slow change over time. For the five years after the most recent epoch, a linear secular-variation model of truncated degree is used for forward extrapolation (NGDC IGRF Web Site). Note that starting with STK-SEET 9.2.3, the IGRF 2010 coefficient set is supported.

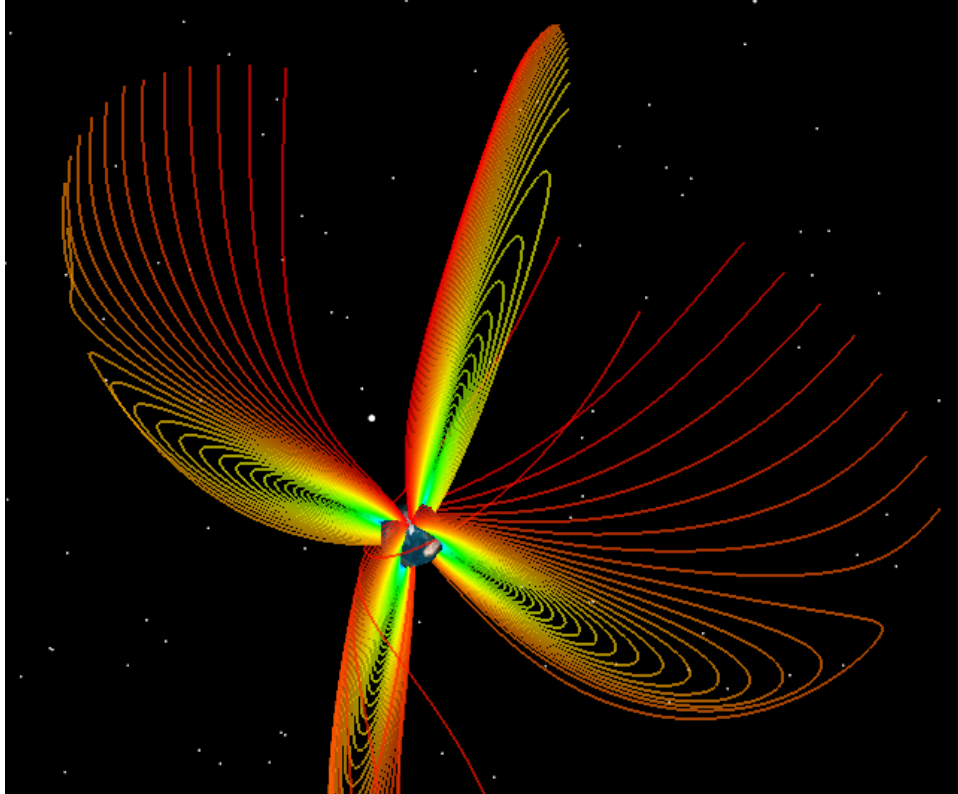


**Figure 6. Sample Magnetic Field Lines showing draping (IGRF with Olson-Pfizer external field).**

In addition to the main field, charged particles emitted from the Sun, called the solar wind, carry the interplanetary magnetic field outward from the Sun in all directions. The solar wind impinges on the Earth's main field, creating a magnetic draping effect that alters the basic dipole character of the near-Earth magnetic field at very high altitudes (Figure 6). The contribution to the magnetic field due to the solar wind interaction is called the *external field* and is modeled separately. The optional external field model for SEET is the *Olson-Pfizer* model (Olson and Pfizer, 1977), which only depends on the local time of one's position of interest within the field (*i.e.*, position relative to the direction of the Sun).

The region in which the Earth's total magnetic field (main and external) exerts the dominant influence on charged particle motions is called the *magnetosphere*. Knowledge of the Earth's magnetic field is useful for satellite engineers and mission planners and operators because the magnetic field largely controls the distributions and motions of high energy charged particles within the magnetosphere: the Van Allen radiation belts, solar energetic particles, and galactic cosmic rays. Such high-energy particles penetrate spacecraft and often cause single event effects and long term degradation of components due to radiation dosing effects (discussed in the Radiation Environment module section above). In low-Earth orbit, measurements of the local magnetic field on a spacecraft in conjunction with knowledge of the model field can also be used for attitude control. The magnetic field also plays a role in electromagnetic radiation propagation, directly for lower-frequencies (Hz-kHz), and indirectly for higher frequencies through its effects on charged particle distributions.

SEET's *Magnetic Field* module computes the full vector magnetic field and magnetic field lines using main-field and external-field model options selected by the user. The range of output is available from the Earth's surface out to a few tens of Earth radii (about 120,000 km). SEET can also compute the dipole  $L$  shell parameter - an identification method for field lines based upon the dipole part of the magnetic field model, the McIlwain  $L$  shell parameter - an identification method for field lines (technically, particle drift shells) computed using adiabatic invariants, and  $B/B_{eq}$  - the ratio of magnetic field strength at the current location to that at the magnetic equator along the same field line. Several Vector Geometry Tool modules are available for computing and visualizing the field, and tools are also available for computing field-line footprints on any altitude surface as well as determining magnetic conjugacy. *Conjugacy* is defined as two spatial locations being connected by the same field-line (to within a small user-specified threshold).

### Main Field Options

*Full-IGRF.* This option provides magnetic field calculations based on the full harmonic expansion of IGRF coefficients. The model coefficients at the epoch of interest are linearly interpolated from the ICRF coefficient tables, the nodes of which are spaced approximately every five years.

*Fast-IGRF.* This option provides a specially tuned version of the IGRF harmonic expansion. It returns a field strength estimate accurate to within 1% of the full-IGRF option, but it is significantly faster (AF-GEOSpace User's Manual Version 2.1P, 2006).

*Tilted-dipole.* (Previously called *centered-dipole*.) The tilted-dipole is an approximation of the Earth's magnetic field with parameters derived from the IGRF coefficient set. The dipole position and orientation is fixed with respect to and collocated at the ECEF coordinate system origin with its axis tilted southward and rotated eastward compared to the ECEF Z and X axes. The IGRF coefficients determine the degree of tilt, which changes gradually over time.

Starting with STK-SEET 9.2.3, the following main field option has been added:

*Offset-dipole.* The offset-dipole is an approximation of the Earth's magnetic field with parameters derived from the IGRF coefficient set. The offset-dipole coordinate system origin is offset by ~500 km from the ECEF coordinate system origin and is tilted such that its dipole axis is parallel to that of the tilted-dipole coordinate system. The IGRF coefficients determine the location and orientation of the coordinate system, which changes gradually over time.

### Other User-Selectable Parameters

*External Field.* The Olson-Pfitzer external field model may be turned on or off. Analyses under about 15000 km altitude generally do not require an external field model. This option can only be used with the *IGRF* and *Fast-IGRF* main field modes.

*IGRF-update rate.* This is the time period of the frequency at which the IGRF model coefficients will be re-evaluated from the table of IGRF coefficients. The default update rate is 1 day, which should be sufficient for most applications. Longer periods may be useful for speeding up calculations involving the magnetic field for longer scenario intervals.

*Field-line refresh rate.* This is the time period of the frequency at which the magnetic field lines will be reconstructed in the solar-magnetic coordinate system using the defined magnetic field model. Longer periods may be useful for speeding up the animated display of magnetic field lines, at the expense of displaying larger step discontinuities in the animated field whenever the

field lines are updated. The default refresh rate of 5 minutes represents a reasonable compromise for most situations.

## APPENDIX A: VERIFICATION OF FLUX MODEL OUTPUTS

**Note:** The following report from Atmospheric and Environmental Research, dated November 2010, documents comparisons of radiation environment flux with other models and provides unit-test outcomes.

Several tests were performed to compare the output from RadEnv with the flux calculated with SPENVIS and IRBEMLIB, two widely used software packages for flux calculations along orbits. Five orbits were selected: LeoInclined, LeoPolar, MeoInclined, MeoLowPerigee and a Molniya orbit. For each orbit integral and differential fluxes were calculated in RadEnv and stored in ASCII files for further processing. Plots were created in Matlab for visual comparison of the outputs. A statistical analysis of the results was also conducted in Matlab. The following statistics were used:

$$\alpha = ((X - Y) / (0.5 * (X + Y)))^2 \quad (1)$$

Here X and Y denote the flux calculated by two of the three different packages (RadEnv, SPENVIS and IRBEMLIB). Four parameters were calculated:  $\min[\sqrt{\alpha}]$ ,  $\max[\sqrt{\alpha}]$ , and  $\text{rms}(\alpha)$ . In calculating these statistics we have ignored cases where either one of the packages or both give -1 for the flux, which means an error. However we have logged these cases and they are under investigation. Also special treatment was given to cases where one of the fluxes is zero but the other one is different from zero. These cases were not included in the statistics given by Eq.1. Instead we calculated a minimum, average and rms for the statistics

$$\delta = \text{abs}(X - Y) \quad (2)$$

Note that this statistic, unlike the one in Eq.1, has a dimension, which is flux in units of ( $\text{cm}^{-2}\text{s}^{-1}$ ).

We also recorded the number of such cases in a separate column. The results from this statistical analysis were organized in tables which are presented below.

### Differential Flux

Since SPENVIS doesn't have an option for calculating differential flux, only a comparison between RadEnv and IRBEMLIB was conducted. First differential fluxes for each orbit were calculated using RadEnv unit tests. The results were stored in ASCII files. Using the download version of IRBEMLIB differential fluxes were generated for the same orbits. The same values for L and B/0 as computed by RadEnv were read from the input file for IRBEMLIB. Since the input values for the magnetic field distribution are the same for both RadEnv and IRBEMLIB, any differences in the calculated flux should be explained by other reasons. Matlab was used to plot the fluxes along the orbits for visual comparison. In addition, Matlab was used to calculate the error statistics described above. The numerical results from this calculation are presented in tables 1-5. In each table the first column is energy in MeV. The next three columns are square root of the minimum error, square root of the maximum error, and rms error for statistics given in Eq.1. The last column shows the total number of cases of the second kind, i.e where one flux is zero and the other is different from zero.

Table 1. LeoInclined, RadEnv vs IRBEMLIB

| Energy (MeV) | MinErr | MaxErr | Rms         | NumErr |
|--------------|--------|--------|-------------|--------|
| 0.65         | 0      | 0.0809 | 0.000440096 | 1      |
| 0.95         | 0      | 0.0934 | 0.000587044 | 1      |
| 1.60         | 0      | 0.0541 | 0.000188615 | 0      |
| 2.00         | 0      | 0.0590 | 0.000224791 | 0      |
| 2.35         | 0      | 0.0638 | 0.000269683 | 0      |
| 2.75         | 0      | 0.1639 | 0.00178933  | 0      |
| 3.15         | 0      | 0.1801 | 0.00215749  | 0      |
| 3.75         | 0      | 0.2024 | 0.0027224   | 0      |
| 4.55         | 0      | 0.2332 | 0.00360217  | 0      |
| 5.75         | 0      | 0.2791 | 0.00514781  | 0      |

Table 2. LeoPolar, RadEnv vs IRBEMLIB

| Energy (MeV) | MinErr | MaxErr | Rms        | NumErr |
|--------------|--------|--------|------------|--------|
| 0.65         | 0      | 0.6934 | 0.0321693  | 0      |
| 0.95         | 0      | 0.3036 | 0.00816027 | 0      |
| 1.60         | 0      | 0.5297 | 0.0209672  | 0      |
| 2.00         | 0      | 0.5868 | 0.0261244  | 0      |
| 2.35         | 0      | 0.6033 | 0.0276586  | 0      |
| 2.75         | 0      | 0.5234 | 0.0189188  | 0      |
| 3.15         | 0      | 0.5736 | 0.0215806  | 0      |
| 3.75         | 0      | 0.6492 | 0.0282555  | 0      |
| 4.55         | 0      | 0.1980 | 0.0050565  | 0      |
| 5.75         | 0      | 0.2382 | 0.00663254 | 0      |

Table 3. MeoInclined, RadEnv vs IRBEMLIB

| Energy (MeV) | MinErr | MaxErr | Rms        | NumErr |
|--------------|--------|--------|------------|--------|
| 0.65         | 0      | 0.9344 | 0.0482165  | 1      |
| 0.95         | 0      | 0.4205 | 0.0158627  | 1      |
| 1.60         | 0      | 0.5300 | 0.0273306  | 1      |
| 2.00         | 0      | 0.5954 | 0.0336319  | 0      |
| 2.35         | 0      | 0.6591 | 0.0481172  | 0      |
| 2.75         | 0      | 0.3154 | 0.0133758  | 0      |
| 3.15         | 0      | 0.2877 | 0.0104563  | 0      |
| 3.75         | 0      | 0.5976 | 0.0215557  | 0      |
| 4.55         | 0      | 0.7433 | 0.0335219  | 0      |
| 5.75         | 0      | 0.3830 | 0.00922434 | 0      |

Table 4. MeoLowPerigee, RadEnv vs IRBEMLIB

| Energy (MeV) | MinErr | MaxErr | Rms        | NumErr |
|--------------|--------|--------|------------|--------|
| 0.65         | 0      | 0.4192 | 0.0254644  | 2      |
| 0.95         | 0      | 0.3406 | 0.0142421  | 2      |
| 1.60         | 0      | 0.3487 | 0.00829317 | 0      |
| 2.00         | 0      | 0.5088 | 0.0139031  | 0      |
| 2.35         | 0      | 0.6520 | 0.0210425  | 0      |
| 2.75         | 0      | 0.5605 | 0.0185723  | 0      |
| 3.15         | 0      | 0.4312 | 0.0181441  | 0      |
| 3.75         | 0      | 0.4739 | 0.0235343  | 0      |
| 4.55         | 0      | 0.2614 | 0.00850499 | 1      |
| 5.75         | 0      | 0.2382 | 0.00663254 | 0      |



Table 5. Molniya, RadEnv vs IRBEMLIB

| Energy (MeV) | MinErr | MaxErr | Rms        | NumErr |
|--------------|--------|--------|------------|--------|
| 0.65         | 0      | 0.5096 | 0.0117665  | 0      |
| 0.95         | 0      | 0.3301 | 0.00444921 | 0      |
| 1.60         | 0      | 0.6939 | 0.0181775  | 0      |
| 2.00         | 0      | 0.2568 | 0.00326018 | 1      |
| 2.35         | 0      | 0.3923 | 0.00835809 | 0      |
| 2.75         | 0      | 0.2847 | 0.00449171 | 0      |
| 3.15         | 0      | 0.2851 | 0.0054136  | 0      |
| 3.75         | 0      | 0.3422 | 0.00708217 | 0      |
| 4.55         | 0      | 0.5554 | 0.0153156  | 0      |
| 5.75         | 0      | 0.2382 | 0.00663254 | 0      |

The minimum error for all orbits is zero, i.e. there are points along all five orbits for which both RadEnv and IRBEMLIB calculate exactly the same electron flux. The maximum error varies from orbit to orbit and is typically of the order of 30-50% with a minimum of 5.4% for the LeoInclined orbit and a maximum of 93% for the MeoInclined orbit. The rms error is typically of the order of a few percent, with the exception of the LeoInclined orbit where the agreement is exceptionally good and the maximum rms error is 0.5%. The number of errors of the second kind is zero for most channels and all orbits. It reaches a maximum of 2 for the first two channels on the MeoLowPerigee orbit. Overall the differential flux calculated from RadEnv is in a very good agreement with the differential flux calculated with IRBEMLIB. For illustration a plot of the flux calculated from RadEnv and IRBEMLIB for the LeoPolar orbit is given in Fig.1

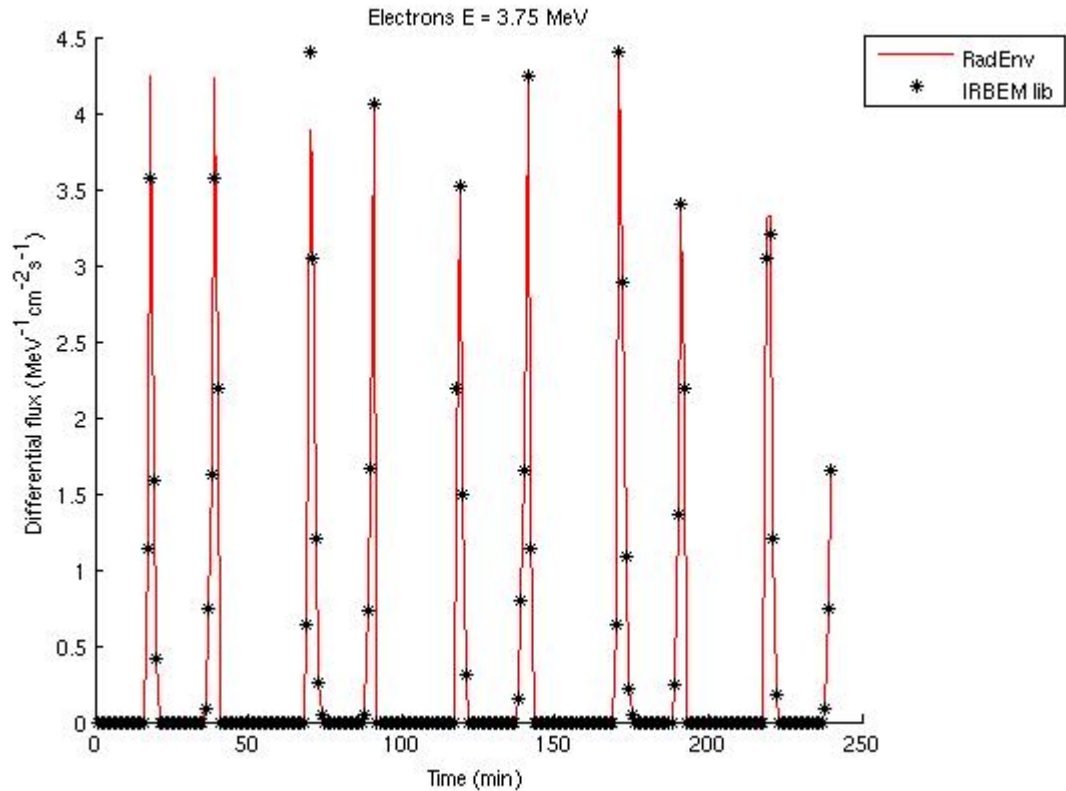


Fig.1 Differential flux calculated by RadEnv and IRBEMLIB along the LeoPolar orbit.

### Integral Flux

The results of the integral flux comparison are organized in plots and tables, similarly to the differential flux comparison. The first column in each table is energy in MeV. The next three columns are square root of the minimum error, square root of the maximum error, and rms error for statistics given in Eq.1.

The last column shows the total number of cases of the second kind, i.e. where one flux is zero and the other is different from zero. In columns 5 and 6 we give minimum, and rms of the error of the second kind, i.e. one of the fluxes is zero the other is different from zero. If the number of such errors in all channels is zero, we skip columns 5 and 6. If the maximum number is one, then we only give the minimum error and skip the rms column.

### SPENVIS comparison

Two flux models, NASA and CRRES were exercised for comparison with SPENVIS. Both proton and electron fluxes were calculated. For the electron flux comparison, the solar activity level was varied between quiet and active ( $A_p = 5$  and  $A_p = 12.5$ ). The output from RadEnv was stored in an ASCII file format for further analysis. Using the online interface of SPENVIS, each orbit was loaded on the server and settings were chosen to match as closely as possible those used in the unit tests. Since SPENVIS does not provide an option for calculating differential flux, only integral fluxes were compared. For each orbit, fluxes were calculated over 240 minute missions for the first two orbits (LeoInclined and LeoPolar) and for 720 minute missions for the other three

(MeoInclined, MeoLowPerigree and Molniya). The calculated fluxes were plotted in Matlab using different colors (blue for SPENVIS output and red for RadEnv output). The plots were organized in HTML files using the Matlab “publish” feature, which creates an HTML document and a number of PNG files (one per energy channel.) The visual comparison shows that the agreement between RadEnv and SPENVIS is good for the LeoInclined, LeoPolar and Molniya orbits. For the two Meo orbits, MeoInclined and MeoLowPerigree, the agreement is not as good. Since the results from RadEnv and SPENVIS were close for two of the orbits but significantly different for the other three it was decided to also compare the integral fluxes from RadEnv with IRBEMlib. Note that since SPENVIS does not allow user input of L and B/B0 values and does not provide B/B0 or B0 in its output, any differences in the underlying magfield models between RadEnv and SPENVIS will contribute to the flux differences. A comparison of differences, for all orbits, in RadEnv and SPENVIS computed L and B values indicates percent differences are less than 1% in all cases, however a systematic analysis of how these differences affect the subsequent flux computations has not been conducted.

### **IRBEMLIB comparison**

Using the Fortran implementation of IRBEMLIB, integral electron fluxes were calculated for the five orbits described in the introduction. The results were stored in ASCII files for further comparison. Matlab was used to read in the data from the ASCII files, to calculate statistics and to plot the flux along the orbit. Plots were stored in HTML files and inspected visually for discrepancies. Statistics were calculated comparing RadEnv with IRBEMLIB, as well as IRBEMLIB with SPENVIS. Results of this comparison are presented in tables below.

### **NASA Flux Model**

For the NASA flux model, only the comparison with SPENVIS was conducted. Errors were computed as described for the differential flux comparisons on page 1. Results are presented in Tables 6-10 below. The minimal error for all orbits is zero and the maximum is 1.24, 1.28, 0.99, 1.47 and 0.95 for the LeoInclined, LeoPolar, MeoInclined, MeoLowPerigree and Molniya orbit. The maximum rms errors are 18%, 15%, 8.7% , 12.6% and 8.3% for these orbits. The maximum number of errors of the second kind for a single channel was 8 for the LeoPolar orbit. For the MeoInclined orbit there were no errors of the second kind in any of the channels.

Table 6. LeoInclined, RadEnv vs SPENVIS (NASAELE model)

| Energy (MeV) | Min-Err | MaxErr | Rms       | MinErr2 | RmsErr2  | NumErr |
|--------------|---------|--------|-----------|---------|----------|--------|
| 0.65/0.7     | 0       | 0.8456 | 0.10577   | 1.412   | 0        | 1      |
| 0.95/1.0     | 0       | 1.2155 | 0.131204  | 1.49697 | 0        | 1      |
| 1.6/1.5      | 0       | 0.9342 | 0.155522  |         |          | 0      |
| 2            | 0       | 0.8421 | 0.0930682 | 1.0024  | 0.516387 | 6      |
| 2.35/2.25    | 0       | 0.9133 | 0.15973   | 1.1909  | 0.206841 | 7      |
| 2.75         | 0       | 0.8972 | 0.110115  | 1.0021  | 0.241622 | 6      |
| 3.15/3.25    | 0       | 0.9629 | 0.137494  | 1.15477 | 0.51392  | 4      |
| 3.75         | 0       | 1.2415 | 0.180027  | 3.4743  | 0        | 1      |
| 4.55/4.5     | 0       | 0      | 0         | 3.0312  | 1.09226  | 3      |
| 5.75/6.0     | 0       | 0      | 0         |         |          | 0      |

Table 7. LeoPolar, RadEnv vs SPENVIS (NASAELE model)

| Energy (MeV) | MinErr | MaxErr | Rms       | MinErr2 | RmsErr2   | NumErr |
|--------------|--------|--------|-----------|---------|-----------|--------|
| 0.65/0.7     | 0      | 1.0622 | 0.134916  | 22.4726 | 0         | 1      |
| 0.95/1.0     | 0      | 1.2853 | 0.150716  | 6.7958  | 0         | 1      |
| 1.6/1.5      | 0      | 0.9254 | 0.10899   | 1.66382 | 0.306527  | 2      |
| 2            | 0      | 0.8750 | 0.0925383 | 1.87699 | 1.35499   | 3      |
| 2.35/2.25    | 0      | 1.0754 | 0.117417  | 1.49391 | 0.0274266 | 2      |
| 2.75         | 0      | 1.0492 | 0.115461  | 1.21706 | 0.248278  | 2      |
| 3.15/3.25    | 0      | 0.9249 | 0.10185   | 1.50585 | 0.402605  | 8      |
| 3.75         | 0      | 0.7815 | 0.0478679 | 1.23956 | 0.153351  | 2      |
| 4.55/4.5     | 0      | 0.4065 | 0.0196971 | 1.27294 | 0.167948  | 2      |
| 5.75/6.0     | 0      | 0.7745 | 0.064579  | 1.96289 | 0.159224  | 4      |

Table 8. MeoInclined, RadEnv vs SPENVIS (NASAELE model)

| Energy (MeV) | MinErr | MaxErr | Rms        | NumErr |
|--------------|--------|--------|------------|--------|
| 0.65/0.7     | 0.0432 | 0.3078 | 0.0201292  | 0      |
| 0.95/1.0     | 0.0394 | 0.3671 | 0.0200399  | 0      |
| 1.6/1.5      | 0.1074 | 0.3837 | 0.0360467  | 0      |
| 2            | 0.0005 | 0.2654 | 0.00156756 | 0      |
| 2.35/2.25    | 0.0462 | 0.3726 | 0.0334759  | 0      |
| 2.75         | 0.0004 | 0.3290 | 0.00299907 | 0      |
| 3.15/3.25    | 0.1087 | 0.9981 | 0.0874085  | 0      |
| 3.75         | 0      | 0.5000 | 0.00527228 | 0      |
| 4.55/4.5     | 0      | 0.3260 | 0.0220713  | 0      |
| 4.55/4.5     | 0      | 0.3260 | 0.0220713  | 0      |

Table 9. MeoLowPerigee, RadEnv vs SPENVIS (NASAELE model)

| Energy (MeV) | MinErr | MaxErr | Rms       | MinErr2 | NumErr |
|--------------|--------|--------|-----------|---------|--------|
| 0.65/0.7     | 0      | 1.2392 | 0.0821507 | 1.58661 | 1      |
| 0.95/1.0     | 0      | 1.4661 | 0.126122  |         | 0      |
| 1.6/1.5      | 0      | 1.2903 | 0.0917914 |         | 0      |
| 2            | 0      | 1.4096 | 0.106519  | 1.31928 | 1      |
| 2.35/2.25    | 0      | 1.3072 | 0.0938553 | 1.0381  | 1      |
| 2.75         | 0      | 1.4285 | 0.108743  | 1.14731 | 1      |
| 3.15/3.25    | 0      | 0.4639 | 0.0248073 | 1.774   | 1      |
| 3.75         | 0      | 0.6041 | 0.0260385 |         | 0      |
| 4.55/4.5     | 0      | 0.3592 | 0.0202952 | 1.04382 | 1      |

Table 10. Molniya, RadEnv vs SPENVIS (NASAELE model)

| Energy (MeV) | MinErr | MaxErr | Rms        | MinErr2 | RmsErr2    | NumErr |
|--------------|--------|--------|------------|---------|------------|--------|
| 0.65/0.7     | 0      | 0.7724 | 0.0355976  | 1.28331 | 1.69332    | 3      |
| 0.95/1.0     | 0      | 0.4359 | 0.0255395  | 1.04654 | 0.295183   | 4      |
| 1.6/1.5      | 0      | 0.6291 | 0.0282018  | 1.1187  | 0          | 1      |
| 2            | 0      | 0.3892 | 0.00791057 | 1.04135 | 0.00570564 | 2      |
| 2.35/2.25    | 0      | 0.5483 | 0.025417   | 1.117   | 0.27061    | 2      |
| 2.75         | 0      | 0.4014 | 0.0126478  |         |            | 0      |
| 3.15/3.25    | 0      | 0.9480 | 0.0830767  |         |            | 0      |
| 3.75         | 0      | 0.5764 | 0.0256887  | 1.16518 | 0          | 1      |
| 4.55/4.5     | 0      | 0.3063 | 0.0176403  | 1.02968 | 0.0819361  | 5      |

A plot illustrating the agreement between the electron fluxes calculated in RadEnv and in SPENVIS for the same threshold energy (2.75 MeV) is given in Fig.2.

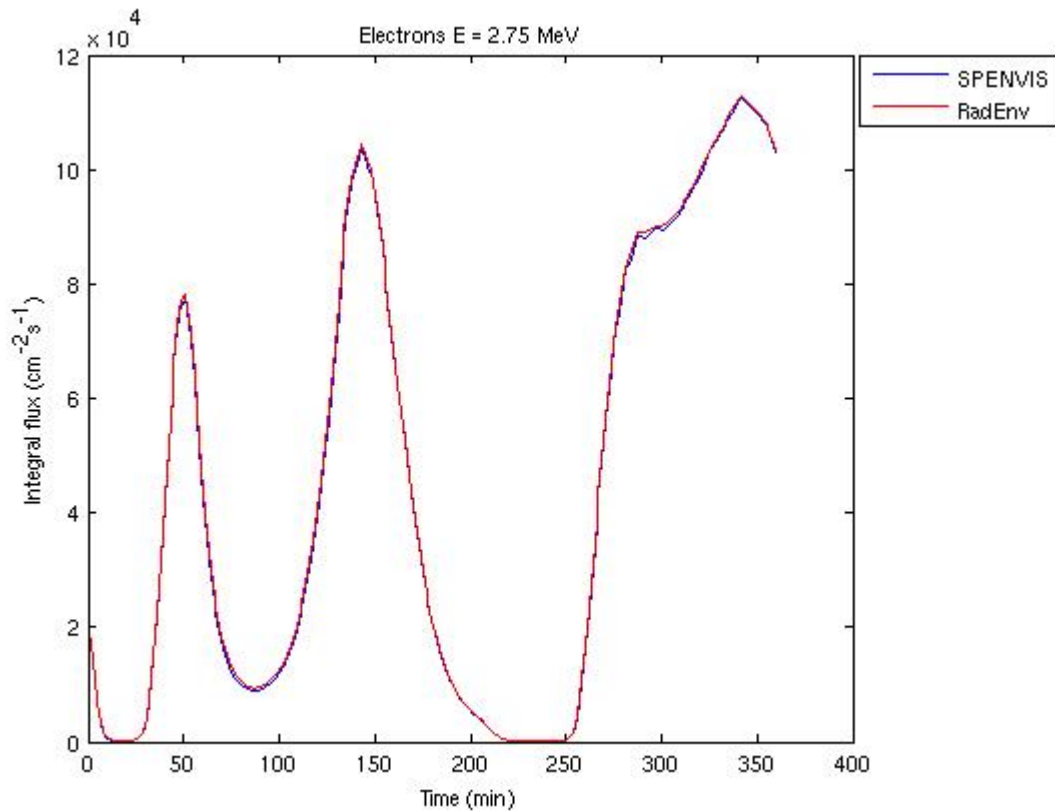


Fig. 2 Integral flux calculated in RadEnv and SPENVIS for the MeoInclined orbit with the NASA flux model.

## CRRES Flux Model

### Results for $A_p = 5$

Solar activity level was first set to  $A_p = 5$ , which corresponds to a quiet Sun. Results are presented in Tables 6- 20. The first column is Energy in RadEnv and IRBEMLIB vs the nearest output energy from SPENVIS. The rest of the columns contain the statistics described in the introduction. The agreement between RadEnv and IRBEMLIB is better than between RadEnv and SPENVIS for all orbits with a few exceptions for some energies. The average error is typically a few percent for the RadEnv/IRBEMLIB comparison, whereas for the RadEnv/SPENVIS comparison it is typically in the several tens of percents or higher.

Table 11. LeoInclined, RadEnv vs IRBEMLib

| Energy (MeV) | MinErr | MaxErr    | Rms        | NumErr |
|--------------|--------|-----------|------------|--------|
| 0.65/0.7     | 0      | 0.128637  | 0.0266517  | 0      |
| 0.95/1.0     | 0      | 0.196856  | 0.0389388  | 0      |
| 1.6/1.5      | 0      | 0.0196051 | 0.00159773 | 0      |
| 2            | 0      | 0.0196051 | 0.00133827 | 0      |
| 2.75         | 0      | 0.0157683 | 0.001413   | 0      |
| 3.15/3.25    | 0      | 0.0218382 | 0.0033323  | 0      |
| 3.75         | 0      | 0.180975  | 0.0134273  | 0      |
| 4.55/4.5     | 0      | 0.376491  | 0.0305441  | 0      |
| 5.75/6.0     | 0      | 0         | 0          | 0      |

Table 12. LeoInclined, RadEnv vs SPENVIS

| Energy (MeV) | MinErr | MaxErr | Rms        | MinErr2  | RmsErr2 | NumErr |
|--------------|--------|--------|------------|----------|---------|--------|
| 0.65/0.7     | 0      | 0.3835 | 0.0107025  |          |         | 0      |
| 0.95/1.0     | 0      | 0.6668 | 0.0363521  |          |         | 0      |
| 1.6/1.5      | 0      | 0.8247 | 0.0588425  |          |         | 0      |
| 2            | 0      | 0.2863 | 0.00758794 |          |         | 0      |
| 2.75         | 0      | 0.4155 | 0.0155707  |          |         | 0      |
| 3.15/3.25    | 0      | 0.8551 | 0.0781444  |          |         | 0      |
| 3.75         | 0      | 0.6544 | 0.0344044  |          |         | 0      |
| 4.55/4.5     | 0      | 0.5866 | 0.0299686  |          |         | 0      |
| 5.75/6.0     | 0      | 0.6744 | 0.0687572  | 0.139425 | 0       | 4      |

Table 13. LeoInclined, IRBEMLib vs SPENVIS

| Energy (MeV) | MinErr | MaxErr | Rms       | NumErr |
|--------------|--------|--------|-----------|--------|
| 0.65/0.7     | 0      | 0.6865 | 0.0424791 | 0      |
| 0.95/1.0     | 0      | 0.9893 | 0.108178  | 0      |
| 1.6/1.5      | 0      | 0.8027 | 0.0543925 | 0      |
| 2            | 0      | 0.3273 | 0.010201  | 0      |
| 2.75         | 0      | 0.4790 | 0.0227375 | 0      |
| 3.15/3.25    | 0      | 0.9476 | 0.105719  | 0      |
| 3.75         | 0      | 0.6105 | 0.028858  | 0      |
| 4.55/4.5     | 0      | 0.5178 | 0.0227264 | 0      |

Table 14. LeoPolar, RadEnv vs IRBEMLib

| Energy (MeV) | MinErr | MaxErr | Rms        | NumErr |
|--------------|--------|--------|------------|--------|
| 0.65/0.7     | 0      | 0.5859 | 0.0294742  | 0      |
| 0.95/1.0     | 0      | 0.6195 | 0.0584263  | 0      |
| 1.6/1.5      | 0      | 0.4863 | 0.0183255  | 0      |
| 2            | 0      | 0.5454 | 0.0210776  | 0      |
| 2.75         | 0      | 0.5001 | 0.0165314  | 0      |
| 3.15/3.25    | 0      | 0.4336 | 0.0221431  | 0      |
| 3.75         | 0      | 0.6492 | 0.0276749  | 0      |
| 4.55/4.5     | 0      | 0.2413 | 0.00867249 | 0      |



Table 15. LeoPolar, RadEnv vs SPENVIS

| Energy (MeV) | MinErr | MaxErr | Rms       | MinErr2  | RmsErr2    | NumErr |
|--------------|--------|--------|-----------|----------|------------|--------|
| 0.65/0.7     | 0      | 0.6462 | 0.0541888 |          |            | 0      |
| 0.95/1.0     | 0      | 0.4703 | 0.0195309 |          |            | 0      |
| 1.6/1.5      | 0      | 1.1608 | 0.185931  |          |            | 0      |
| 2            | 0      | 0.9922 | 0.183068  |          |            | 0      |
| 2.75         | 0      | 0.9371 | 0.118426  |          |            | 0      |
| 3.15/3.25    | 0      | 0.9776 | 0.211953  |          |            | 0      |
| 3.75         | 0      | 0.7036 | 0.0847522 | 0.0212   | 0.00617954 | 4      |
| 4.55/4.5     | 0      | 0.4804 | 0.0317364 |          |            | 0      |
| 5.75/6.0     | 0      | 0.6423 | 0.0286356 | 0.025575 | 0.0684354  | 31     |

Table 16. LeoPolar, IRBEMLib vs SPENVIS

| Energy (MeV) | MinErr | MaxErr | Rms       | MinErr2 | RmsErr2    | NumErr |
|--------------|--------|--------|-----------|---------|------------|--------|
| 0.65/0.7     | 0      | 0.6295 | 0.0617741 |         |            | 0      |
| 0.95/1.0     | 0      | 0.6711 | 0.093984  |         |            | 0      |
| 1.6/1.5      | 0      | 1.0833 | 0.139159  |         |            | 0      |
| 2            | 0      | 0.8945 | 0.137233  |         |            | 0      |
| 2.75         | 0      | 0.9252 | 0.121947  |         |            | 0      |
| 3.15/3.25    | 0      | 1.1725 | 0.313453  |         |            | 0      |
| 3.75         | 0      | 0.6881 | 0.0787713 | 0.01652 | 0.00903265 | 4      |
| 4.55/4.5     | 0      | 0.5826 | 0.0457663 |         |            | 0      |

Table 17. MeoInclined, RadEnv vs IRBEMLib

| Energy (MeV) | MinErr | MaxErr | Rms        | NumErr |
|--------------|--------|--------|------------|--------|
| 0.65/0.7     | 0      | 0.5646 | 0.0449722  | 0      |
| 0.95/1.0     | 0      | 0.5895 | 0.0688361  | 0      |
| 1.6/1.5      | 0      | 0.3734 | 0.0213155  | 0      |
| 2            | 0      | 0.3545 | 0.022417   | 0      |
| 2.75         | 0      | 0.3145 | 0.00798687 | 0      |
| 3.15/3.25    | 0      | 0.3325 | 0.0176876  | 0      |
| 3.75         | 0      | 0.4678 | 0.0232669  | 0      |
| 4.55/4.5     | 0      | 1.0279 | 0.121508   | 0      |

Table 18. MeoInclined, RadEnv vs SPENVIS

| Energy (MeV) | MinErr | MaxErr | Rms       | MinErr2 | RmsErr2   | NumErr |
|--------------|--------|--------|-----------|---------|-----------|--------|
| 0.65/0.7     | 0      | 0.4900 | 0.0811462 |         |           | 0      |
| 0.95/1.0     | 0      | 0.3680 | 0.0132891 |         |           | 0      |
| 1.6/1.5      | 0      | 0.8603 | 0.23515   |         |           | 0      |
| 2            | 0      | 0.8228 | 0.218327  |         |           | 0      |
| 2.75         | 0      | 0.7529 | 0.113838  |         |           | 0      |
| 3.15/3.25    | 0      | 0.8450 | 0.225085  |         |           | 0      |
| 3.75         | 0      | 1.1840 | 0.227129  |         |           | 0      |
| 4.55/4.5     | 0      | 0.3530 | 0.0236861 | 0.16904 | 0         | 1      |
| 5.75/6.0     | 0      | 0.9323 | 0.202628  | 0.16904 | 0.0805642 | 2      |

Table 19. MeoInclined, IRBEMLib vs SPENVIS

| Energy (MeV) | MinErr | MaxErr | Rms      | NumErr |
|--------------|--------|--------|----------|--------|
| 0.65/0.7     | 0      | 0.4704 | 0.069521 | 0      |
| 0.95/1.0     | 0      | 0.7052 | 0.106274 | 0      |
| 1.6/1.5      | 0      | 0.7143 | 0.144446 | 0      |
| 2            | 0      | 0.6762 | 0.130726 | 0      |
| 2.75         | 0      | 0.6943 | 0.101594 | 0      |
| 3.15/3.25    | 0      | 1.0186 | 0.310921 | 0      |
| 3.75         | 0      | 1.0811 | 0.190081 | 0      |
| 4.55/4.5     | 0      | 1.0787 | 0.127886 | 0      |

Table 20. MeoLowPerigee, RadEnv vs IRBEMLib

| Energy (MeV) | MinErr | MaxErr | Rms       | NumErr |
|--------------|--------|--------|-----------|--------|
| 0.65/0.7     | 0      | 0.4075 | 0.0268837 | 0      |
| 0.95/1.0     | 0      | 0.5545 | 0.069753  | 0      |
| 1.6/1.5      | 0      | 0.4723 | 0.0177235 | 0      |
| 2            | 0      | 0.6347 | 0.0251311 | 0      |
| 2.75         | 0      | 0.4304 | 0.012613  | 0      |
| 3.15/3.25    | 0      | 0.3697 | 0.0228359 | 0      |
| 3.75         | 0      | 0.4994 | 0.0267692 | 0      |
| 4.55/4.5     | 0      | 1.0986 | 0.134088  | 0      |

Table 21. MeoLowPerigee, RadEnv vs SPENVIS

| Energy (MeV) | MinErr | MaxErr | Rms       | MinErr2  | RmsErr2   | NumErr |
|--------------|--------|--------|-----------|----------|-----------|--------|
| 0.65/0.7     | 0      | 0.7949 | 0.105586  |          |           | 0      |
| 0.95/1.0     | 0      | 0.4494 | 0.0234429 |          |           | 0      |
| 1.6/1.5      | 0      | 1.2907 | 0.276449  |          |           | 0      |
| 2            | 0      | 1.2671 | 0.255     |          |           | 0      |
| 2.75         | 0      | 0.8865 | 0.125142  |          |           | 0      |
| 3.15/3.25    | 0      | 1.0527 | 0.232127  |          |           | 0      |
| 3.75         | 0      | 1.2803 | 0.212911  | 0.0252   | 0.0166508 | 5      |
| 4.55/4.5     | 0      | 1.2422 | 0.0734938 | 0.17647  | 0.0973757 | 2      |
| 5.75/6.0     | 0      | 0.8066 | 0.134243  | 0.025575 | 0.0441063 | 64     |

Table 22. MeoLowPerigee, IRBEMLib vs SPENVIS

| Energy (MeV) | MinErr | MaxErr | Rms       | MinErr2 | RmsErr2   | NumErr |
|--------------|--------|--------|-----------|---------|-----------|--------|
| 0.65/0.7     | 0      | 0.7442 | 0.0938418 |         |           | 0      |
| 0.95/1.0     | 0      | 0.8032 | 0.123683  |         |           | 0      |
| 1.6/1.5      | 0      | 1.1793 | 0.212689  |         |           | 0      |
| 2            | 0      | 1.1551 | 0.185033  |         |           | 0      |
| 2.75         | 0      | 0.9575 | 0.128757  |         |           | 0      |
| 3.15/3.25    | 0      | 1.1873 | 0.335649  |         |           | 0      |
| 3.75         | 0      | 1.2079 | 0.207479  | 0.02504 | 0.0168743 | 5      |
| 4.55/4.5     | 0      | 1.5264 | 0.147395  |         |           | 0      |

Table 23. Molniya, RadEnv vs IRBEMLib

| Energy (MeV) | MinErr | MaxErr | Rms        | NumErr |
|--------------|--------|--------|------------|--------|
| 0.65/0.7     | 0      | 0.4906 | 0.0159124  | 0      |
| 0.95/1.0     | 0      | 0.5689 | 0.0432713  | 0      |
| 1.6/1.5      | 0      | 0.5308 | 0.0137862  | 0      |
| 2            | 0      | 0.3891 | 0.0115975  | 0      |
| 2.75         | 0      | 0.3260 | 0.00584521 | 0      |
| 3.15/3.25    | 0      | 0.4290 | 0.0133964  | 0      |
| 3.75         | 0      | 0.4030 | 0.00916925 | 0      |
| 4.55/4.5     | 0      | 1.0393 | 0.0437455  | 0      |

Table 24. Molniya, RadEnv vs SPENVIS

| Energy (MeV) | MinErr | MaxErr | Rms        | MinErr2  | RmsErr2  | NumErr |
|--------------|--------|--------|------------|----------|----------|--------|
| 0.65/0.7     | 0      | 0.5440 | 0.0394806  |          |          | 0      |
| 0.95/1.0     | 0      | 0.2991 | 0.00741982 |          |          | 0      |
| 1.6/1.5      | 0      | 1.0215 | 0.134246   |          |          | 0      |
| 2            | 0      | 0.9519 | 0.116121   |          |          | 0      |
| 2.75         | 0      | 0.9742 | 0.0582831  |          |          | 0      |
| 3.15/3.25    | 0      | 0.9741 | 0.133086   |          |          | 0      |
| 3.75         | 0      | 0.8227 | 0.0579184  |          |          | 0      |
| 4.55/4.5     | 0      | 0.3436 | 0.0111177  | 0.30592  |          | 1      |
| 5.75/6.0     | 0      | 0.9356 | 0.0941251  | 0.025575 | 0.101795 | 8      |

Table 25. Molniya, IRBEMLib vs SPENVIS

| Energy (MeV) | MinErr | MaxErr | Rms       | NumErr |
|--------------|--------|--------|-----------|--------|
| 0.65/0.7     | 0      | 0.5305 | 0.0429312 | 0      |
| 0.95/1.0     | 0      | 0.6228 | 0.0680477 | 0      |
| 1.6/1.5      | 0      | 0.9353 | 0.0953008 | 0      |
| 2            | 0      | 0.8636 | 0.0782401 | 0      |
| 2.75         | 0      | 0.9976 | 0.0610951 | 0      |
| 3.15/3.25    | 0      | 1.1508 | 0.194171  | 0      |
| 3.75         | 0      | 0.8231 | 0.0498631 | 0      |
| 4.55/4.5     | 0      | 1.1226 | 0.0506694 | 0      |

One example plot of the fluxes calculated by RadEnv, IRBEMLIB and SPENVIS is given in Fig. 3 Note that the agreement between RadEnv and IRBEMLIB is considerably better than between either one of these software packages and SPENVIS. Note that the intermittent dropouts in the RadEnv data here and below have been resolved with a bug-fix update.

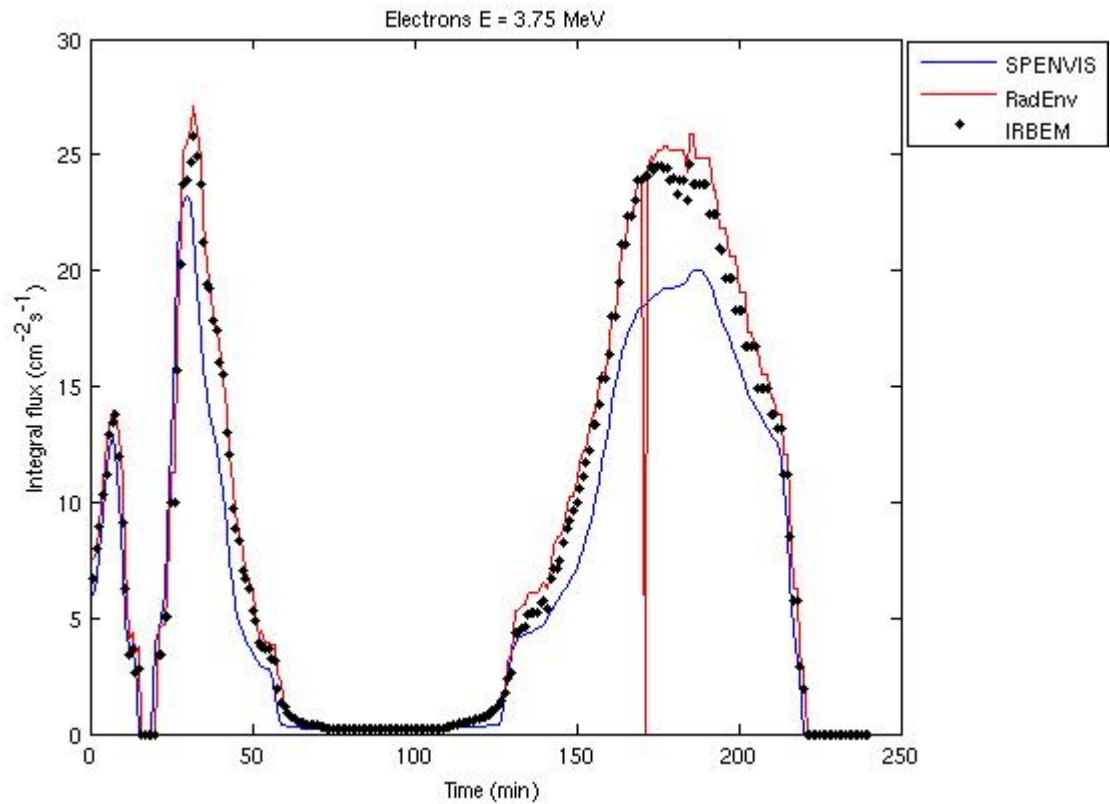


Fig.3 Integral flux calculated in RadEnv, SPENVIS and IRBEMLIB for the MeoInclined orbit with the CRRESEL flux model. Activity Ap index is 5 for IRBEMLIB and 5 – 7.5 for SPENVIS. Note: The drop-out near 170 minutes has since been fixed.

## Results for Ap = 12.5

Initially, before fixing some of the bugs, a poor agreement between RadEnv and SPENVIS integral fluxes was observed for some of the orbits, particularly the two Meo orbits, and for some of the energy channels. This prompted a new calculation at a different solar activity level. SPENVIS gives as a choice a range of activity levels. For this study, it was set to 12.5 in RadEnv. In SPENVIS activity level was set to 10-15 for the CRRESEL model. In IRBEMLIB the parameter A15 was set to 12.5.

Overall the agreement between RadEnv and SPENVIS is slightly worse at the higher activity level. For the MeoInclined orbit at Ap = 5 the highest rms error is 23.5%, whereas at Ap = 12.5 it is 44%. The maximum error for Ap=5 is 1.18 whereas for Ap=12.5 it is 1.48.

Table 26. LeoInclined, RadEnv vs IRBEMLib

| Energy (MeV) | MinErr | MaxErr | Rms        | NumErr |
|--------------|--------|--------|------------|--------|
| 0.65/0.7     | 0      | 0.1931 | 0.00362741 | 0      |
| 0.95/1.0     |        | 0.2342 | 0.00958356 | 0      |
| 1.6/1.5      | 0      | 0.2207 | 0.00379993 | 0      |
| 2            | 0      | 0.2319 | 0.0038178  | 0      |
| 2.75         | 0      | 0.2294 | 0.00353869 | 0      |
| 3.15/3.25    | 0      | 0.2566 | 0.00461331 | 0      |
| 3.75         | 0      | 0.3909 | 0.0118102  | 0      |
| 4.55/4.5     | 0      | 0.6275 | 0.0381235  | 0      |

Table 27. LeoInclined, RadEnv vs SPENVIS

| Energy (MeV) | MinErr | MaxErr | Rms        | NumErr |
|--------------|--------|--------|------------|--------|
| 0.65/0.7     | 0      | 0.9521 | 0.163201   | 0      |
| 0.95/1.0     | 0      | 0.4494 | 0.017849   | 0      |
| 1.6/1.5      | 0      | 0.6764 | 0.0457756  | 0      |
| 2            | 0      | 0.6840 | 0.0451387  | 0      |
| 2.75         | 0      | 0.4435 | 0.0188579  | 0      |
| 3.15/3.25    | 0      | 0.5378 | 0.0393918  | 0      |
| 3.75         | 0      | 0.4446 | 0.0245001  | 0      |
| 4.55/4.5     | 0      | 0.1742 | 0.00295181 | 0      |
| 5.75/6.0     | 0      | 0.3579 | 0.0146263  | 0      |

Table 28. LeoInclined, IRBEMLib vs SPENVIS

| Energy (MeV) | MinErr | MaxErr | Rms       | NumErr |
|--------------|--------|--------|-----------|--------|
| 0.65/0.7     | 0      | 0.8725 | 0.133871  | 0      |
| 0.95/1.0     | 0      | 0.6291 | 0.0442534 | 0      |
| 1.6/1.5      | 0      | 0.6109 | 0.034374  | 0      |
| 2            | 0      | 0.6428 | 0.0378955 | 0      |
| 2.75         | 0      | 0.4766 | 0.0233029 | 0      |
| 3.15/3.25    | 0      | 0.5941 | 0.0526781 | 0      |
| 3.75         | 0      | 0.4036 | 0.0173986 | 0      |
| 4.55/4.5     | 0      | 0.4184 | 0.0214023 | 0      |

Table 29. LeoPolar, RadEnv vs IRBEMLib

| Energy (MeV) | MinErr | MaxErr | Rms        | NumErr |
|--------------|--------|--------|------------|--------|
| 0.65/0.7     | 0      | 0.2469 | 0.00526684 | 0      |
| 0.95/1.0     | 0      | 0.4791 | 0.054528   | 0      |
| 1.6/1.5      | 0      | 0.4865 | 0.0177244  | 0      |
| 2            | 0      | 0.5448 | 0.0213117  | 0      |
| 2.75         | 0      | 0.5118 | 0.0186674  | 0      |
| 3.15/3.25    | 0      | 0.4498 | 0.0251734  | 0      |
| 3.75         | 0      | 1.5152 | 0.188607   | 0      |
| 4.55/4.5     | 0      | 0.4444 | 0.0211655  | 0      |

Table 30. LeoPolar, RadEnv vs SPENVIS

| Energy (MeV) | MinErr | MaxErr | Rms       | MinErr2  | RmsErr2   | NumErr |
|--------------|--------|--------|-----------|----------|-----------|--------|
| 0.65/0.7     | 0      | 0.8259 | 0.0940271 |          |           | 0      |
| 0.95/1.0     | 0      | 0.3325 | 0.013028  |          |           | 0      |
| 1.6/1.5      | 0      | 0.8615 | 0.1122    |          |           | 0      |
| 2            | 0      | 0.8268 | 0.122123  |          |           | 0      |
| 2.75         | 0      | 0.6969 | 0.0623956 |          |           | 0      |
| 3.15/3.25    | 0      | 1.0106 | 0.195454  |          |           | 0      |
| 3.75         | 0      | 1.2634 | 0.277215  |          |           | 0      |
| 4.55/4.5     | 0      | 0.6397 | 0.0714718 | 0.064325 | 0         | 2      |
| 5.75/6.0     | 0      | 1.3700 | 0.252247  | 0.025575 | 0.0791207 | 25     |

Table 31. LeoPolar, IRBEMLib vs SPENVIS

| Energy (MeV) | MinErr | MaxErr | Rms       | NumErr |
|--------------|--------|--------|-----------|--------|
| 0.65/0.7     | 0      | 0.7348 | 0.0857305 | 0      |
| 0.95/1.0     | 0      | 0.6411 | 0.0895401 | 0      |
| 1.6/1.5      | 0      | 0.7705 | 0.079885  | 0      |
| 2            | 0      | 0.7864 | 0.0941882 | 0      |
| 2.75         | 0      | 0.7273 | 0.0764811 | 0      |
| 3.15/3.25    | 0      | 1.1554 | 0.284389  | 0      |
| 3.75         | 0      | 1.2293 | 0.284201  | 0      |
| 4.55/4.5     | 0      | 0.8205 | 0.117969  | 0      |

Table 32. MeoInclined, RadEnv vs IRBEMLib

| Energy    | MinErr | MaxErr | Rms        | NumErr |
|-----------|--------|--------|------------|--------|
| 0.65/0.7  | 0      | 0.1746 | 0.00507187 | 0      |
| 0.95/1.0  | 0      | 0.4409 | 0.060397   | 0      |
| 1.6/1.5   | 0      | 0.2891 | 0.0158162  | 0      |
| 2         | 0      | 0.2948 | 0.0175693  | 0      |
| 2.75      | 0      | 0.2389 | 0.00721638 | 0      |
| 3.15/3.25 | 0      | 0.2597 | 0.0135226  | 0      |
| 3.75      | 0      | 0.3351 | 0.0202071  | 0      |
| 4.55/4.5  | 0      | 0.5760 | 0.0596506  | 0      |



Table 33. MeoInclined, RadEnv vs SPENVIS

| Energy (MeV) | MinErr | MaxErr | Rms       | MinErr2 | RmsErr2   | NumErr |
|--------------|--------|--------|-----------|---------|-----------|--------|
| 0.65/0.7     | 0      | 0.9473 | 0.163742  |         |           | 0      |
| 0.95/1.0     | 0      | 0.5025 | 0.0389207 |         |           | 0      |
| 1.6/1.5      | 0      | 0.6973 | 0.12448   |         |           | 0      |
| 2            | 0      | 0.7397 | 0.130393  |         |           | 0      |
| 2.75         | 0      | 0.5742 | 0.0664218 |         |           | 0      |
| 3.15/3.25    | 0      | 0.9032 | 0.212868  |         |           | 0      |
| 3.75         | 0      | 1.0927 | 0.26882   |         |           | 0      |
| 4.55/4.5     | 0      | 0.6069 | 0.0735496 |         |           | 0      |
| 5.75/6.0     | 0      | 1.3232 | 0.443173  | 0.09735 | 0.0235666 | 30     |

Table 34. MeoInclined, IRBEMLib vs SPENVIS

| Energy (MeV) | MinErr | MaxErr | Rms       | NumErr |
|--------------|--------|--------|-----------|--------|
| 0.65/0.7     | 0      | 0.8730 | 0.138051  | 0      |
| 0.95/1.0     | 0      | 0.7252 | 0.111774  | 0      |
| 1.6/1.5      | 0      | 0.6774 | 0.0794003 | 0      |
| 2            | 0      | 0.6532 | 0.0843382 | 0      |
| 2.75         | 0      | 0.5406 | 0.0682738 | 0      |
| 3.15/3.25    | 0      | 1.0360 | 0.281526  | 0      |
| 3.75         | 0      | 1.0010 | 0.242468  | 0      |
| 4.55/4.5     | 0      | 0.6940 | 0.0960998 | 0      |

Table 35. MeoLowPerigee, RadEnv vs IRBEMLib

| Energy    | MinErr | MaxErr | Rms        | NumErr |
|-----------|--------|--------|------------|--------|
| 0.65/0.7  | 0      | 0.2577 | 0.00669368 | 0      |
| 0.95/1.0  | 0      | 0.5457 | 0.0609334  | 0      |
| 1.6/1.5   | 0      | 0.4150 | 0.0167822  | 0      |
| 2         | 0      | 0.3976 | 0.0191059  | 0      |
| 2.75      | 0      | 0.4911 | 0.0139816  | 0      |
| 3.15/3.25 | 0      | 0.5505 | 0.0235801  | 0      |
| 3.75      | 0      | 0.8093 | 0.0405363  | 0      |
| 4.55/4.5  | 0      | 1.1028 | 0.0706691  | 0      |

Table 36. MeoLowPerigee, RadEnv vs SPENVIS

| Energy (MeV) | MinErr | MaxErr | Rms       | MinErr2  | RmsErr2    | NumErr |
|--------------|--------|--------|-----------|----------|------------|--------|
| 0.65/0.7     | 0      | 0.8768 | 0.102932  |          |            | 0      |
| 0.95/1.0     | 0      | 0.6406 | 0.0421943 |          |            | 0      |
| 1.6/1.5      | 0      | 1.4034 | 0.202127  |          |            | 0      |
| 2            | 0      | 1.4763 | 0.212627  |          |            | 0      |
| 2.75         | 0      | 1.2911 | 0.166711  |          |            | 0      |
| 3.15/3.25    | 0      | 1.3529 | 0.273232  |          |            | 0      |
| 3.75         | 0      | 1.1564 | 0.283273  |          |            | 0      |
| 4.55/4.5     | 0      | 0.6519 | 0.0767744 | 0.064325 | 0.00876674 | 12     |
| 5.75/6.0     | 0      | 1.3900 | 0.524724  | 0.025575 | 0.0958572  | 84     |

Table 37. MeoLowPerigee, IRBEMLib vs SPENVIS

| Energy (MeV) | MinErr | MaxErr | Rms       | MinErr2 | RmsErr2    | NumErr2 |
|--------------|--------|--------|-----------|---------|------------|---------|
| 0.65/0.7     | 0      | 0.8972 | 0.0912046 |         |            | 0       |
| 0.95/1.0     | 0      | 1.0091 | 0.126433  |         |            | 0       |
| 1.6/1.5      | 0      | 1.3487 | 0.153192  |         |            | 0       |
| 2            | 0      | 1.4266 | 0.162287  |         |            | 0       |
| 2.75         | 0      | 1.3177 | 0.144527  |         |            | 0       |
| 3.15/3.25    | 0      | 1.4212 | 0.329384  |         |            | 0       |
| 3.75         | 0      | 1.2299 | 0.265417  |         |            | 0       |
| 4.55/4.5     | 0      | 0.8119 | 0.123677  | 0.0186  | 0.00963062 | 12      |

Table 38. Molniya, RadEnv vs IRBEMLib

| Energy    | MinErr | MaxErr | Rms        | NumErr |
|-----------|--------|--------|------------|--------|
| 0.65/0.7  | 0      | 0.2028 | 0.00255098 | 0      |
| 0.95/1.0  | 0      | 0.6154 | 0.0427866  | 0      |
| 1.6/1.5   | 0      | 0.4058 | 0.00946628 | 0      |
| 2         | 0      | 0.4060 | 0.00976059 | 0      |
| 2.75      | 0      | 0.4498 | 0.00840248 | 0      |
| 3.15/3.25 | 0      | 0.6866 | 0.0210512  | 0      |
| 3.75      | 0      | 1.5152 | 0.0864181  | 0      |
| 4.55/4.5  | 0      | 0.7488 | 0.0463985  | 0      |

Table 39. Molniya, RadEnv vs SPENVIS

| Energy (MeV) | MinErr | MaxErr | Rms        | MinErr2 | RmsErr2   | NumErr2 |
|--------------|--------|--------|------------|---------|-----------|---------|
| 0.65/0.7     | 0      | 0.8162 | 0.0609619  |         |           | 0       |
| 0.95/1.0     | 0      | 0.2815 | 0.00683589 |         |           | 0       |
| 1.6/1.5      | 0      | 0.7924 | 0.0667493  |         |           | 0       |
| 2            | 0      | 0.8369 | 0.0707911  |         |           | 0       |
| 2.75         | 0      | 0.6656 | 0.0292557  |         |           | 0       |
| 3.15/3.25    | 0      | 1.0377 | 0.114372   |         |           | 0       |
| 3.75         | 0      | 1.2510 | 0.153155   |         |           | 0       |
| 4.55/4.5     | 0      | 0.5898 | 0.0296377  |         |           | 0       |
| 5.75/6.0     | 0      | 1.2882 | 0.233359   | 0.04455 | 0.0278504 | 17      |

Table 40. Molniya, IRBEMLib vs SPENVIS

| Energy    | MinErr | MaxErr | Rms       | NumErr2 |
|-----------|--------|--------|-----------|---------|
| 0.65/0.7  | 0      | 0.8071 | 0.060533  | 0       |
| 0.95/1.0  | 0      | 0.6773 | 0.0613514 | 0       |
| 1.6/1.5   | 0      | 0.7034 | 0.0407489 | 0       |
| 2         | 0      | 0.7525 | 0.0450479 | 0       |
| 2.75      | 0      | 0.7220 | 0.0345752 | 0       |
| 3.15/3.25 | 0      | 1.2121 | 0.16889   | 0       |
| 3.75      | 0      | 1.2526 | 0.138828  | 0       |
| 4.55/4.5  | 0      | 0.9645 | 0.069087  | 0       |

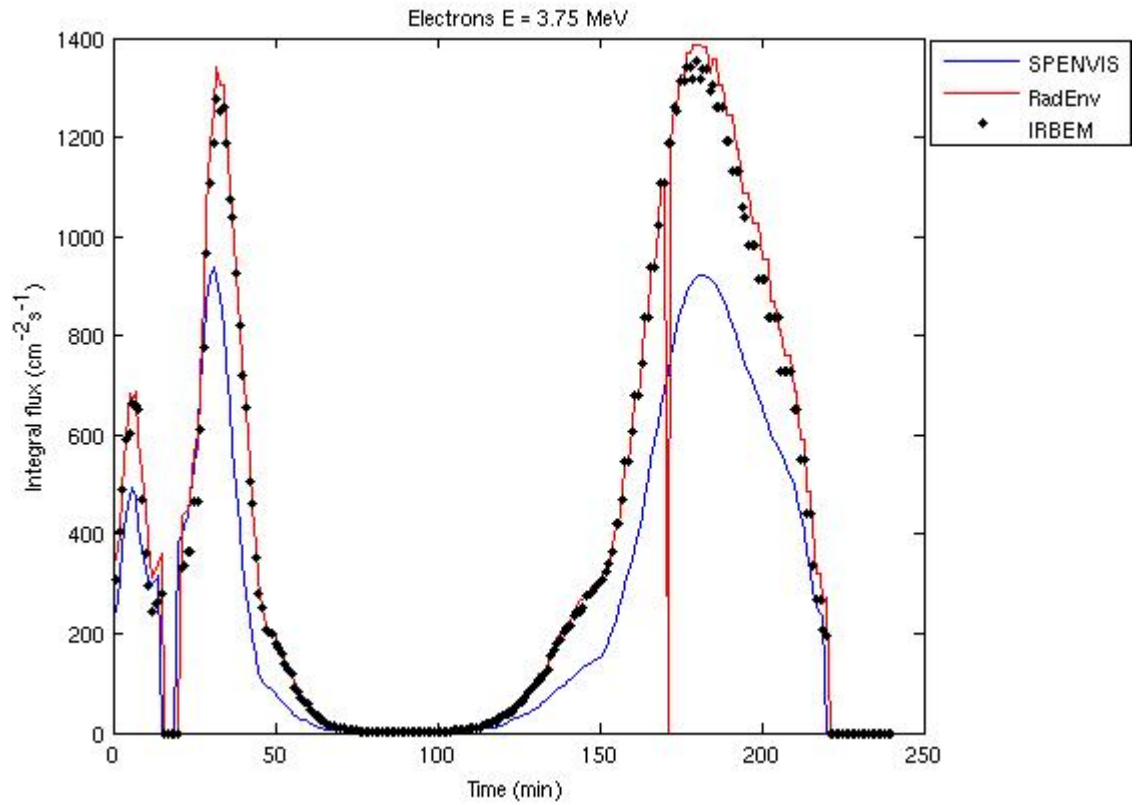


Fig.4 Integral flux calculated in RadEnv, SPENVIS and IRBEMLIB for the MeoInclined orbit with the CRRESEL flux model. Activity Ap index is 12.5 for IRBEMLIB and 10-15 for SPENVIS. *Note: The drop-out near 170 minutes has since been fixed.*

## APPENDIX B: REFERENCES

- Adams, J. H., Jr, (1987), *Cosmic Ray Effects on Microelectronics, Part IV*. NRL Memo Rep. 5901, Naval Research Laboratory, Washington, DC.
- AF-GEOSpace User's Manual Version 2.1 and 2.1P, AFRL/RVBS, 29 Randolph Rd, Hanscom AFB, MA 01731 (2006).
- AFSPC Pamphlet 15-2, *Space Environmental Impacts on DOD Operations*, October 2003.
- Badhwar, G. D., and P. M. O'Neill (1996), "Galactic cosmic radiation model and its applications." *Adv. Space Res.*, vol. 17, no. 2, pp. (2)7–(2)17.
- Beck, P., M. Latocha, S. Rollet, and G. Stehno (2005), TEPC reference measurements at aircraft altitudes during a solar storm, *Adv. Space Res.*, 36, 1627–1633.
- Bell, J.T., and M.S. Gussenhoven (1997), *APEX RAD Documentation*. PL-TR-97-2117, AD 331633.
- Bourdarie, S., and M. Xapsos (2008), "The Near-Earth Space Radiation Environment," *IEEE Trans. Nucl. Sci.*, vol 55, No. 4, pp 1810 – 1832. doi: 10.1109/TNS.2008.2001409
- Brautigam, D.H., and J. Bell (1995), CRRESELE Documentation, PL-TR-95-2128. Phillips Laboratory, Hanscom AFB, MA, ADA 301770.
- Cunningham, F.G. (1961), "Earth Reflected Solar Radiation Input to Spherical Satellites." NASA Technical Note D-1099.
- Cunningham, F.G. (1963), "Earth Reflected Solar Radiation Incident Upon an Arbitrarily Oriented Spinning Flat Plate", NASA Technical Note, D-1842.
- Dyer, C. S., K. Hunter, S. Clucas, and A. Campbell (2004), Observation of the solar particle events of October and November 2003 from CREDO and MPTB, *IEEE Trans. Nucl. Sci.*, 51(6), 3388 --3393, doi:10.1109/TNS.2004.839156.
- FAA Website, Environmental Control and Life-support Subsystem (ECLSS), Section 4.4.1.3, Basic Principles of Thermal Control.
- Feynman, J., and S.B. Gabriel (2000), "On space weather consequences and predictions." *J. Geophys. Res.*, 105(A5), 10543–10564, doi:10.1029/1999JA000141.
- Feynman, J., G. Spitale, J. Wang, and S. Gabriel (1993), "Interplanetary Proton Fluence Model: JPL 1991," *J. Geophysics. Res.*, 98, 13281.
- Feynman J., A. Ruzmaikin, and V. Berdishevsky (2002), "The JPL proton fluence model: an update." *JASTP*, 64, 1679.
- Fraser-Smith, A.C. (1987), "Centered and Eccentric Geomagnetic Dipoles and Their Poles, 1600-1985." *Rev. of Geophysics*, No. 1, pp. 1-16.
- Ginet, G.P., D. Madden, B.K. Dichter and D.H. Brautigam (2007), "Energetic Proton Maps for the South Atlantic Anomaly." *IEEE Radiation Effects Data Workshop*, 23-27 July 2007.
- Getley, I. L., M. L. Duldig, D. F. Smart, and M. A. Shea (2005a), Radiation dose along North American transcontinental flight paths during quiescent and disturbed geomagnetic conditions, *Space Weather*, 3, S01004, doi:10.1029/2004SW000110.
- Glover, A.; Hilgers, A.; Rosenqvist, L.; Bourdarie, S., "Interplanetary proton cumulated fluence model update," *Advances in Space Research*, Volume 42, Issue 9, p. 1564-1568, 2007.
- Griffin, M.D., J.R. French (1991), *Space Vehicle Design*. American Institute of Aeronautics and Astronautics, Inc.
- Grun, E., Zook, H.A., Fechtig, H. Geise, R.H., (1985), "Collisional Balance of the Meteoritic Complex." *Icarus*, v. 62, p. 244.
- Heirtzler, J.R., "The Future of the South Atlantic anomaly and implications for radiation damage in space," *Journal of Atmospheric and Solar-Terrestrial Physics*, v. 64, p. 1701-08 (2002).

- Heynderickx, D., J. Lemaire, E. J. Daly and H. D. R. Evans (1996), "Calculating Low-Altitude Trapped Particle Fluxes with the NASA Models AP-8 and AE-8." *Radiation Measurements*, Vol. 26, pp. 947-952.
- Huston, S.L., G.A. Kuck, and K.A. Pfitzer (1996), "Low altitude trapped radiation model using TIROS/NOAA data, in Radiation Belts: Models and Standards." J.F. Lemaire, D. Heynderickx, and D.N. Baker (eds.), *Geophysical Monograph 97*, American Geophysical Union, 119.
- ISO, "Space environment (natural and artificial) -- Galactic cosmic ray model," ISO 15390:2004.
- Jenniskens, P. (1994), "Meteor stream activity: I. The Annual Streams." *Astronomy and Astrophysics*, 287, 990-1013.
- Kearns, K.J. and M.S. Gussenhoven (1992), CRRESRAD Documentation, PL-TR-92-2201, Phillips Laboratory, Hanscom AFB, MA, ADA 256673.
- Kessler, D. J., Watts, A. J., Crowell, J. (1989), "Orbital Debris Environment for Spacecraft Designed to Operate in Low Earth Orbit." NASA TM-100-471.
- Love, S. G., and D. E. Brownlee (1993), "A Direct Measurement of the Terrestrial Mass Accretion Rate of Cosmic Dust, Science." v. 262, pp. 550-53.
- McDonnell, J.A.M., K. Sullivan (1992), "Hypervelocity Impacts on Space Detectors: Decoding the Projectile Parameters." In *Hypervelocity Impacts in Space*, ed. J.A.M. McDonnell (Canterbury: University of Kent), pp 39-47.
- McNeil, W. (1999), "Problems in the Prediction of Meteor Shower Effects on the Atmosphere", 37<sup>th</sup> AIAA Aerospace Sciences Meeting and Exhibit, January 1999, Reno, NV.
- McNeil, W.J., R.A. Dressler, E. Murad (2001), "Impact of a Major Meteor Storm on Earth's Ionosphere: A Modeling Study", *Journal of Geophysical Research*, 106, 10,447-10,465.
- Meffert, J.D., and M.S. Gussenhoven, CRRESPRO Documentation, PL-TR-94-2218, Phillips Laboratory, Hanscom AFB, MA (1994), ADA 284578.
- NASA Preferred Reliability Practice Guideline, "Earth Orbit Environmental Heating," No. GD-AP-2301. National Aeronautics and Space Administration, Goddard Space Flight Center, Greenbelt, MD.
- NASA National Space Science Data Center (NSSDC) website URL: <ftp://nssdcftp.gsfc.nasa.gov/>.
- NGDC Web Site, International Geomagnetic Reference Field URL: <http://www.ngdc.noaa.gov/IAGA/vmod/igrf.html>
- Nymmik, R.A. (2000) "Time lag of galactic cosmic ray modulation: Conformity to general regularities and influence on particle energy spectra," *Adv. Space Res.*, v. 26, no. 11, pp. 1875–2000.
- O'Neill, P. M. (2006), "Badhwar-O'Neill galactic cosmic ray model update based on Advanced Composition Explorer (ACE) energy spectra from 1997 to present," *Adv. Space Res.*, vol. 37, pp. 1727–1733.
- O'Neill, P. M. (2010), "Badhwar–O'Neill 2010 Galactic Cosmic Ray Flux Model – Revised," *IEEE Trans. Nucl. Sci.*, vol. 57, no. 6, pp 3148 – 3153; doi: 10.1109/TNS.2010.2083688.
- Olson, W.P. and K.A. Pfitzer (1977), Magnetospheric magnetic field modeling, Annual Scientific Report, AFOSR Contract No. F44620-75-C-0033.
- Rendtel, J., Arlt, R., McBeath, A. (eds., 1995). *Handbook for Visual Meteor Observers*. The International Meteor Organization, Potsdam, Germany.
- Rosenqvist, L., Hilgers, A., Evans, H., Daly, E., Hapgood, M., Stamper, R., Zwickl, R., Bourdarie, S., Boscher, D. "Toolkit for updating interplanetary proton-cumulated fluence models." *J. Spacecraft Rockets*, 42(6), 1077 - 1090, 2005.
- Seltzer, S.M. (1994), "Updated Calculations for Routine Space-Shielding Radiation Dose Estimates: SHIELDOSE-2." National Institute of Standards and Technology Publication NISTIR 5477.
- "Space Station Freedom Natural Environment Definition for Design" (1991), NASA SSP 30425 Rev. A, Chap. 8.
- SPENVIS System Website, Background on Magnetic Field Models. (<http://www.spenvis.oma.be/spenvis/help/background/magfield/magfield.html>)
- Stevenson, J.A. and J.C. Crafton (1961), "Radiation Heat Transfer Analysis for Space Vehicles", ASD Technical Report 61-119.

Tribble, A.C. (1995), "The Space Environment: Implications for Spacecraft Design." Princeton Univ. Press, Princeton, p. 24.

Tsyganenko, N.A., A Magnetospheric Magnetic Field Model with a Warped Tail Current Sheet, *Planet. Space Sci.*, 37, 5-20 (1989).

Xapsos, M. A., J. L. Barth, E. G. Stassinopoulos, E. A. Burke, and G. B. Gee, Space Environment Effects: Model for Emission of Solar Protons (ESP)—Cumulative and Worst-Case Event Fluences, NASA/TP-1999-209763, Marshall Space Flight Center, AL, 1999.

Xapsos, M.A., C. Stauffer, T. Jordan, J.L. Barth, R. A. Mewaldt (2007), "Model for Cumulative Solar Heavy Ion Energy and Linear Energy Transfer Spectra." *IEEE Trans. Nucl. Sci.*, vol. 54, pp 1085-1989.

Xapsos, M.A., G.P. Summers, J. L. Barth, and E. G Stassinopoulos (2000), "Probability Model for Cumulative Solar Proton Fluences." *IEEE Trans. Nucl. Sci.*, vol. 47, pp 486-490.

Xapsos, M.A., P.M. O'Neill, and T.P. O'Brien (2013), "Near-Earth Space Radiation Models." *IEEE Trans. Nucl. Sci.*, vol. 60, no. 3, pp 1691-1705; doi: 10.1109/TNS.2012.2225846.